Kara, J., Väisänen, M., Heinonen, J. S., Lahaye, Y., O'Brien, H., & Huhma, H., 2020. Tracing arclogites in the Paleoproterozoic Era–A shift from 1.88 Ga calc-alkaline to 1.86 Ga high-Nb and adakite-like magmatism in central Fennoscandian Shield. Lithos, 372, 105663. https://doi.org/10.1016/j.lithos.2020.105663


# Tracing arclogites in the Paleoproterozoic Era – a shift from 1.88 Ga calc-alkaline to 1.86 Ga high-Nb and adakite-like magmatism in central Fennoscandian Shield

Jaakko Kara[a*], Markku Väisänen[a], Jussi S. Heinonen[b], Yann Lahaye[c], Hugh O'Brien[c], Hannu Huhma[c]
[a] *Department of Geography and Geology, University of Turku, Turku, Finland*
[b] *Department of Geosciences and Geography, University of Helsinki, Helsinki, Finland*
[c] *Geological Survey of Finland, Espoo, Finland*
* *Corresponding author: jkmkar@utu.fi (Jaakko Kara)*

Abstract
Arclogites, i.e., lower crustal garnet-pyroxenite cumulates, are suggested to play an important role in controlling magma differentiation in modern continental arcs. Until now, arclogite-related magmatism has only been described from the Phanerozoic Era. The Svecofennian orogen in the central Fennoscandian Shield hosts a rare association of 1.86 Ga igneous rocks geochemically distinct from the surrounding and much more abundant 1.90–1.87 Ga subduction-related calc-alkaline magmatism. The 1.86 Ga magmatic rocks are divided into three groups: 1) high-Nb gabbros (HNB) which are enriched in $Fe_2O_3^T$, $TiO_2$, $P_2O_5$, F, LILE, and HFSE (especially Nb; 18.9–44 ppm), show positive initial $\varepsilon_{Nd}$ value, and near-chondritic but variable initial zircon $\varepsilon_{Hf}$ values; 2) high-Mg gabbros (HMG) which are characterised by high MgO, CaO, Cr and Ni contents, slight enrichment in LILE, positive $\varepsilon_{Nd}$, and positive but variable zircon $\varepsilon_{Hf}$ values; 3) adakite-like rocks showing high $Al_2O_3$ and $Na_2O$ contents, slight enrichment in LILE, relative depletion in some HFSE, positive $\varepsilon_{Nd}$ value, and chondritic to negative zircon $\varepsilon_{Hf}$ values. The three groups yield zircon U-Pb ages of ~1.86 Ga and exhibit undeformed textures in contrast to the surrounding supracrustal rocks metamorphosed at ~1.88 Ga. The ages and compositions are clearly different from the adjacent 1.90–1.87 Ga arc-related igneous rocks suggesting a distinct origin. Despite similar ages and close spatial relationship, separate sources are required for each of the different 1.86 Ga rock groups. Trace element modelling of partial melting suggests that arclogites, with compositions similar to pyroxenite xenoliths found in the kimberlite pipes of eastern Finland, are the source for the HNB rocks. In contrast, subduction-modified mantle peridotite is the source for the HMG rocks, and a mafic lower crustal source is suggested for the adakite-like rocks. The following geodynamic model is suggested: (rutile-bearing) arclogite formation at 1.90–1.87 Ga followed by arclogite delamination and partial melting during extension of the thickened Svecofennian crust at 1.86 Ga.

Keywords: Arclogite; High-Nb gabbro; Svecofennian orogen; Geochemistry; Sm-Nd isotopes; Zircon U-Pb-Hf isotopes

## 1. Introduction

The majority of volcanic arc magmas are suggested to originate by partial melting of metasomatised peridotite in the mantle wedge (e.g., Tatsumi et al., 1986; Hawkesworth et al., 1993). However, melting of peridotite alone cannot explain the whole compositional spectrum of mafic magmas encountered in magmatic arcs (e.g., Tatsumi, 2000; Castillo, 2012). Increasing evidence suggests that pyroxenites could play an important role not only in intraplate environments, such as in the generation of ocean island basalts (OIB; Sobolev et al., 2005; Herzberg, 2011, 2014), but also within arc environments (Lee et al., 2006, 2007).

A peculiar rock group reported from modern arcs is high-Nb basalts (Reagan and Gill, 1989) which erupt in a convergent margin environment, but show compositions similar to intraplate alkaline basalts enriched in large ion lithophile elements (LILE), light rare earth elements (LREE) and some other high field strength elements (HFSE), especially Nb (>20ppm) (e.g., Castillo, 2008; Hastie et

al., 2011). Petrogenesis of these high-Nb basalts is still controversial. Reagan & Gill (1989) proposed that a small-degree partial melting of a source similar to those of OIB and subsequent interaction with high-degree partial melts of depleted upper mantle is responsible for the characteristic incompatible trace element patterns (see Castillo, 2008, 2012). Another model is based on the occurrence of high-Nb basalts together with rocks derived by melting of young and hot subducted slab (Defant et al., 1992), i.e., adakites (Defant and Drummond, 1990). In that scenario Defant et al. (1992) and Kepezhinskas et al. (1995) suggested interaction of slab melt with mantle wedge, which would produce Nb-rich amphibole and subsequent partial melting of this metasomatic mantle would then be the source for high-Nb basalts.

Recently, Tang et al. (2019) suggested that delamination and partial melting of deep arc garnet-pyroxenite cumulates could explain the Nb-Ta systematics of small-volume intracontinental basalts. These pyroxenites, or "arclogites" (Anderson, 2005), are distinguished from common subduction-related eclogites by their mineral composition since they are not omphacite-rich and do not have an oceanic crustal protolith. The model of arclogite formation and delamination within a 20–30 Ma time span (Lee et al., 2006, 2007; Lee & Anderson, 2015) is based on 1) well-known imbalance between the composition of average continental crust and magmatism in modern arcs (e.g., Kay and Kay, 1988; Rudnick, 1995), 2) fractional crystallisation of basaltic primary magma to form mafic cumulates (gabbros to garnet-pyroxenites) and complementary felsic melts in subduction zones (Kay and Kay, 1993; Tatsumi, 2000; Tang et al., 2018), and 3) field observations of Mesozoic garnet-pyroxenite cumulate xenoliths within the Sierra Nevada batholiths (Ducea & Saleeby, 1996; Wernicke et al., 1996; Zandt et al., 2004). Experimental studies have shown that partial melting of garnet-pyroxenites can produce alkaline and OIB-like magmas (Hirschmann et al., 2003; Kogiso et al., 2003) and delaminated pyroxenites have been suggested to be a significant source for OIBs (McKenzie & O'Nions, 1983; Tatsumi, 2000). Moreover, Tang et al. (2019) showed that in intracrustal environments, crustal thickness (=pressure) controls the Nb/Ta fractionation in magmas. This is explained by rutile crystallisation in arclogites so that the greater the crustal thickness the higher the Nb/Ta in arclogites and, subsequently, the lower the Nb/Ta in arc magmas. On the other hand, partial melting of such rutile-bearing arclogites would produce magmas with elevated Nb/Ta.

To date, arclogites have been described only from modern continental margin settings. In this study, we extend the arclogite model to the Paleoproterozoic Era. We report modal compositions, whole-rock major and trace element and Sm-Nd isotopic compositions, zircon and monazite U-Pb ages and zircon Hf isotopes from rare 1.86 Ga high-Nb gabbros (HNB), high magnesium gabbros (HMG) and adakite-like rocks in the Svecofennian orogen, central Fennoscandia. These data are compared to the surrounding 1.90–1.87 Ga continental arc-type rocks from the area. We suggest a model of formation, delamination and partial melting of arclogites to describe the evolution and shift from ~1.88 Ga magmatism to the 1.86 Ga magmatism and use mantle melt modelling to understand the source characteristics of the 1.86 Ga magmas. In addition, the arclogite-model is used to explain the formation of the extremely thick crust and the high velocity lower crust encountered in the central Fennoscandian Shield.

## 2. Geological setting

### *2.1. Svecofennian orogen*

The Paleoproterozoic Svecofennian orogen (SO) in the central Fennoscandian Shield of the East European Craton (Gorbatschev & Bogdanova, 1993) is separated from the Archean Karelian Province by a NW-SE striking major shear zone (Fig. 1a; Koistinen, 1981). The SO in Finland is suggested to consist of at least three stacked terranes which were accreted to the Archean craton during the Svecofennian orogeny: the Savo belt, Central Svecofennia and Southern Svecofennia. Central Svecofennia can be further divided into the granitoid-dominated Central Finland Granitoid Complex,

Kara, J., Väisänen, M., Heinonen, J. S., Lahaye, Y., O'Brien, H., & Huhma, H., 2020. Tracing arclogites in the Paleoproterozoic Era–A shift from 1.88 Ga calc-alkaline to 1.86 Ga high-Nb and adakite-like magmatism in central Fennoscandian Shield. Lithos, 372, 105663. https://doi.org/10.1016/j.lithos.2020.105663 (Author's postprint)

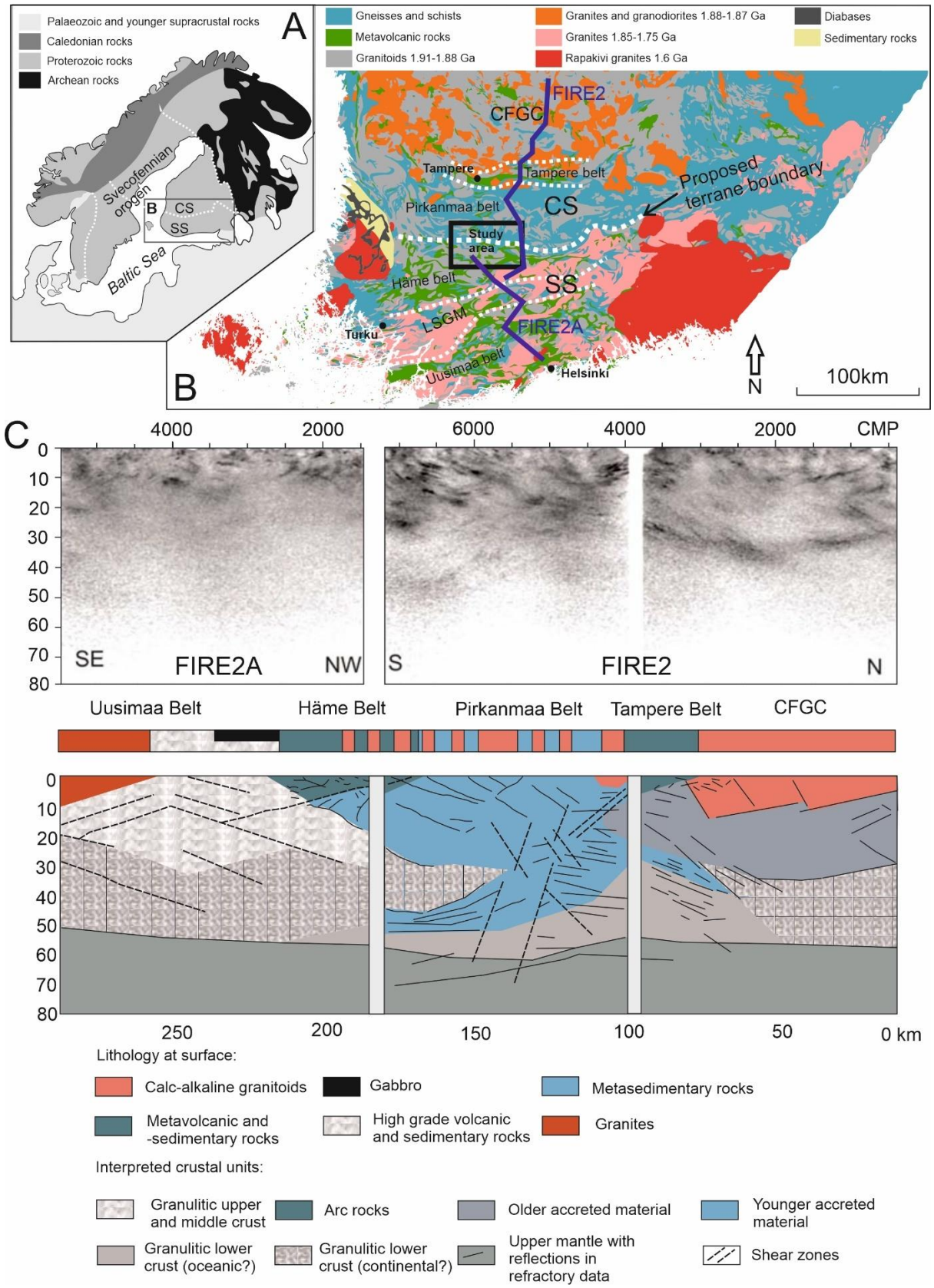


Fig. 1. a) Geological overview of the Fennoscandian Shield modified after Koistinen et al. (2001). b) Lithological map of southern Finland modified after Bedrock of Finland - DigiKP. The study area is indicated by a black rectangle. c) Deep seismic reflection profiles FIRE2 and FIRE2A and interpretations. Depth in kilometres and distance in common mid-points (CMPs) and kilometres. No vertical exaggeration. Modified after Lahtinen et al. (2009a). CFGC = Central Finland Granitoid Complex, CS = Central Svecofennia, SS = Southern Svecofennia, LSGM = Late Svecofennian granite-migmatite zone.

the lower amphibolite facies volcano/sedimentary Tampere belt and higher amphibolite sedimentary Pirkanmaa belt. Southern Svecofennia is characterised by two E-W trending volcanic belts, the lower amphibolite Häme belt in the north and higher amphibolite facies Uusimaa belt in the south (Fig. 1b; Korsman et al., 1997; Kähkönen, 2005; Lahtinen et al., 2009a).

The SO is characterised by up to 60-km-thick crust in eastern and south-central Finland (Fig. 1c; Luosto, 1991). Lahtinen et al. (2005) suggested a microcontinent accretion against the Archean continent at 1.92–1.87 Ga followed by an extensional phase between 1.87 and 1.84 Ga prior to the continent-continent collision at 1.84–1.79 Ga. An alternative view was presented by Rutland et al. (2004), Hermansson et al. (2008) and Stephens & Andersson (2015) in which subduction beneath a single active continental margin in combination with hinge retreat and advance resulted in switching between contractional and extensional tectonics (Hermansson et al., 2008). In both models, an extensional phase occurred at 1.87–1.84 Ga; this is supported by the existence of ultra-mature lateritic paleosols between the basement rocks and quartzites of this age in southern Finland and central Sweden. These findings coupled with structural and geophysical interpretations indicate the opening of several rift basins during an extensional tectonic regime (e.g., Bergman et al., 2008).

The extremely thick crust in the SO is interpreted to result from magmatic underplating (Stephens & Andersson, 2015) or as a combination of tectonic thickening and post-collisional magmatic underplating (e.g., Korja et al., 1993; Kukkonen et al., 2006; Lahtinen et al., 2009a). The mechanism and causes for the thickening have also been speculated based on studies of lower crustal xenoliths hosted by the Kaavi kimberlite pipes. The xenoliths comprise garnet pyroxenites, mafic garnet granulites, hornblendites and gabbros (Hölttä et al., 2000) with a subpopulation of eclogitic garnet and clinopyroxene xenocrysts (Kukkonen et al., 2008). Although located within the Archean terrane in eastern Finland, Peltonen et al. (2006) showed that the growth of the mafic granulite layer took place in several stages, the 1.9 Ga accretion of the Svecofennian arc complexes being the most important one. Kukkonen et al. (2008) suggested formation of a 5–30 km thick eclogitic high velocity lower crust (HVLC) during the early Svecofennian orogeny at 1.91–1.87 Ga beneath the Central Finland Granitoid Complex, and delamination of the HVLC during the late orogenic stage at ~1.85 Ga.

Mantle-derived magmatism was continuous during the entire orogenic cycle in southern Finland (e.g., Rutanen et al., 2011; Kara et al., 2018). The 1.87–1.84 Ga magmatism is relatively rare in the Svecofennian rock record, but recent studies have confirmed both felsic and mafic magmatism in southern Finland and central Sweden at the time. Väisänen et al. (2012a) and Nevalainen et al. (2014) reported 1.865–1.85 Ga mafic intrusions in SW Finland. These show enrichment in Fe, Ti, P, F, LILE and LREE and geochemical affinity to within-plate setting. Similar ages have been inferred for mafic dykes in east-central Sweden (Hermansson et al., 2008; Dahlin et al., 2014; Johansson & Karlsson, 2020). The compositions of these dykes are variable, but they are suggested to reflect the possible extensional tectonics during the intra-orogenic stage of the SO. In the Central Finland Granitoid Complex, an age of ~1.87 Ga has been suggested for a few Fe-Ti-P rich gabbros based on field relations with the post-kinematic ~1.87 Ga granites (Nironen et al., 2000; Rämö et al., 2001). However, one of these gabbros yielded an age of 1.88 Ga (Kärkkäinen et al., 1999) suggesting that they may have a diverse origin (Peltonen, 2005). Moreover, Halkoaho et al. (2020) reported an age of 1.86 Ga for a small granite-gabbro association in the north-eastern margin of the Central Finland Granitoid Complex. In addition, 1.87 Ga TTG- or adakite-like rocks, suggested to derive from high pressure partial melting of mafic lower crust, have been found in southern Finland (Väisänen et al., 2012b; Ruotoistenmäki, 2019).

### *2.2. Study area*

The study area straddles the proposed terrane boundary between Central and Southern Svecofennia (Lahtinen, 1994; Korsman et al., 1997; Fig. 1b and 2). The northern part of it within Central Svecofennia consists of the Pirkanmaa belt sedimentary and plutonic rocks (Kilpeläinen, 1998; Kähkönen, 2005). The Pirkanmaa belt is dominated by migmatitised psammitic gneisses of turbiditic origin deposited at 1.92–1.89 Ga (Huhma et al., 1991; Kähkönen, 2005; Lahtinen et al., 2009b). It also includes minor ultramafic to mafic volcanic rocks with MORB to WPL affinities (Peltonen, 1995; Lahtinen, 1996; Kähkönen, 2005), small ultramafic to mafic intrusions with arc or transitional MORB affinities (Peltonen, 1995, 2005) and various synorogenic granitoids (Nironen & Bateman, 1989). The granitoids within the Pirkanmaa belt comprise 1.89–1.87 Ga tonalites, quartz diorites and granodiorites (Nironen & Bateman, 1989; Nironen, 2005). North of the Pirkanmaa belt, the Tampere belt is characterised by volcanic rocks formed in an active continental margin 1.91–1.89 Ga ago (Kähkönen, 2005).The Pirkanmaa belt is interpreted as a mid-crustal expression of an accretionary prism of the Tampere belt volcanic arc complex (Lahtinen, 1996; Kähkönen, 2005).

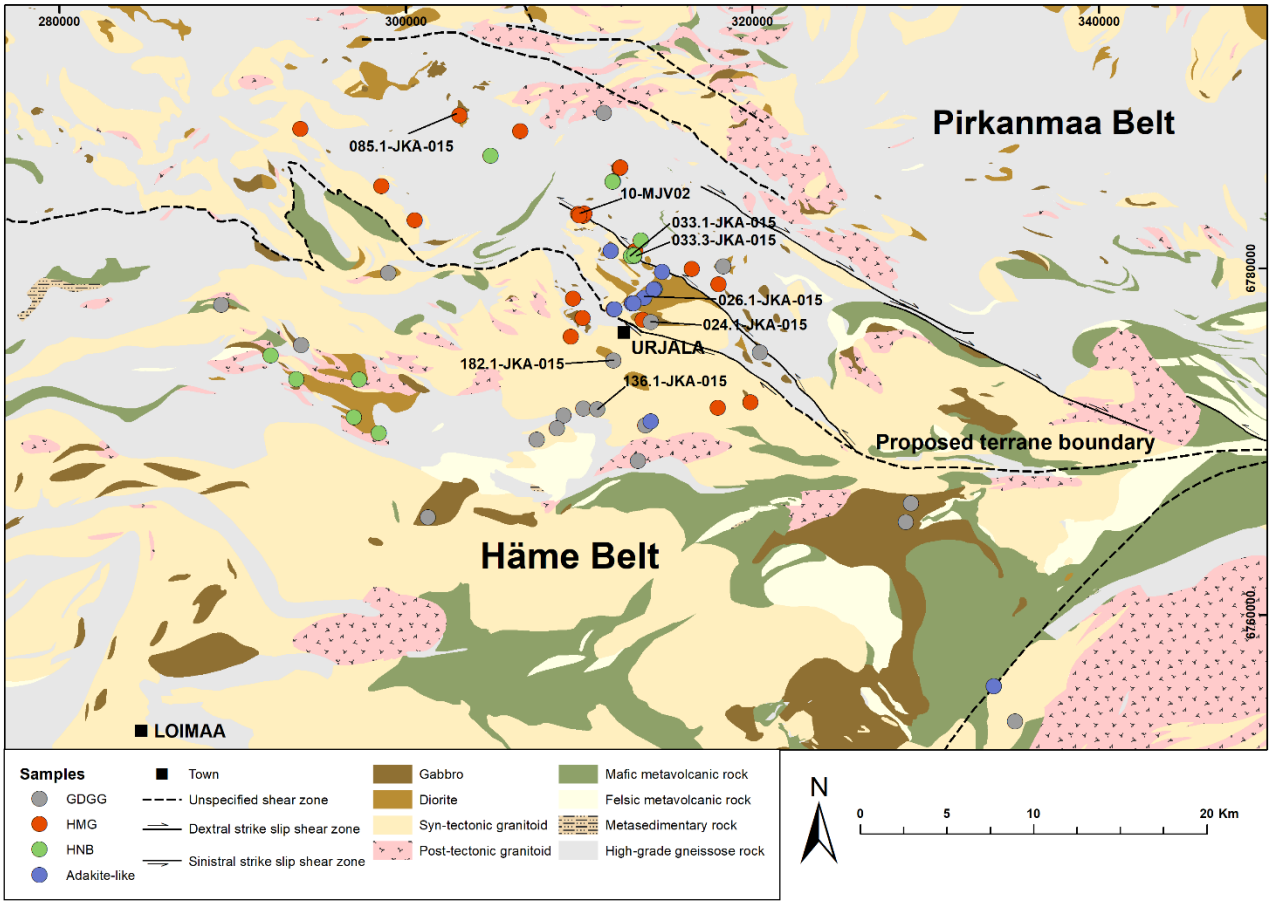


Fig. 2. Simplified lithological map of the study area with sampling sites indicated. Modified after Bedrock of Finland – DigiKP.

The southern part of the study area, the 1.89–1.88 Ga Häme belt within Southern Svecofennia, consists of mafic, intermediate and felsic volcanic and plutonic rocks emplaced in a subduction-related volcanic arc environment (Fig. 1b and 2; Lahtinen, 1996; Kähkönen, 2005). Granitoids are abundant and mostly occur as large 1.89–1.88 Ga intrusions (Mäkitie et al., 2016). Also, a few younger plutons, dated at 1.87 Ga but considered as synorogenic, have been reported from the western part of the Häme belt (Nironen, 2005). The mafic plutonic rocks show similar ~1.88 Ga ages to synorogenic felsic intrusives (Patchett & Kouvo, 1986; Suominen, 1988). The volcanic rocks in the

NE part of the Häme belt show rift-related characteristics whereas in the central parts they are arc-related (Lahtinen, 1996; Kähkönen, 2005).

## 3. Methods

Whole-rock geochemical analyses were performed at Acme Analytical Laboratories Ltd. (Acme) in Vancouver, Canada by inductively coupled plasma-optical emission spectrometry (ICP-OES; major elements, Sc and F) and by inductively coupled plasma-mass spectrometry (ICP-MS; other trace elements). Back-scattered electron (BSE) images and mineral identification of the zircons, monazites and baddeleyites were done using a JEOL JSM-7100F FE-SEM equipped with EDS analyser in the Finnish Geosciences Research Laboratory (SGL) at the Geological Survey of Finland, Espoo. Zircon and monazite U-Pb ages were performed by Nu Plasma HR multicollector or AttoM single collector ICP-MS analysers at SGL. Whole-rock Sm-Nd isotope analyses were carried out at SGL using a standard liquid sample introduction system involving nebulizer, a DSN and a Nu Plasma HR multicollector ICP-MS. Zircon Hf isotope analyses were carried out using the Nu Plasma HR multicollector ICP-MS at SGL. The full analytical description can be found in Electronic Appendix A.

## 4. Results

### *4.1. Sample description, modal compositions and major and trace element geochemistry*

The complete major and trace element and Nd isotopic data are available in Electronic Appendix B. The 67 analysed samples were divided into four groups based on field observations, geochemistry, age and mineralogy: 1) high-Mg gabbros (HMG, n=21), 2) high-Nb gabbros (HNB, n=14), 3) adakite-like rocks (n=11) and 4) 1.90–1.87 Ga subduction-related calc-alkaline gabbro-diorite-granodiorite-granite series rocks (GDGG, n=21). Modal composition was determined for a representative sample from each group except for the GDGG series since it represents multiple rock types. A summary of the whole-rock geochemistry and modal compositions are presented in Table 1.

#### *4.1.1. Gabbro-diorite-granodiorite-granite series*

The GDGG contains intrusive rocks from the adjacent Pirkanmaa and Häme belts (Fig. 2). The rocks occur as slightly deformed mafic to felsic plutons which support their syntectonic nature exhibiting magma mingling in places.

The GDGG samples range from gabbros to granites within the calc-alkaline and high-K calc-alkaline magma series (Fig. 4a). In the immobile trace element classification diagram (Fig. 4b), the samples spread across the basalt, andesite, basaltic andesite, trachyandesite, rhyolite, dacite and trachyte fields. They show a uniform trend in decreasing MgO, $Fe_2O_3^T$, CaO, $TiO_2$ and increasing alkali content with increasing silica content (Fig. 5).

The samples show a variable but increasing trend in Rb, Ba and Zr with increasing silica contents, whereas Cr, Ni and Y decrease slightly and Sr, Nb and F stay rather constant (Fig. 6). The GDGG series shows a clear negative anomaly in Nb-Ta, P and Ti but enrichment in the subduction-mobile elements such as Rb, Ba, Th, Pb and LREE (Fig. 7a). The REE patterns are fractionated (LREE-enriched) and show negative Eu anomalies (Fig. 7b).

#### *4.1.2. High-Mg gabbros*

The HMG occur as WNW-ESE-striking dykes or small elongated intrusions with lengths of tens to hundreds of meters and widths of few to tens of metres. The dykes crosscut the surrounding migmatitic metasedimentary country rocks, apparently dipping gently to the NNE. The dykes are undeformed, but the country rock is partially melted at the upper contact and tonalitic back-veining from the country rock into the gabbro dykes is common (Fig. 3). The contacts lack chilled margins,

but grain size variation from fine-grained contact zones to medium-grained interiors is observed. The HMG exhibit an ophitic to subophitic texture of Ca-plagioclase laths with intergranular magmatic hornblende (Fig. 3). Other phases are biotite (both primary and secondary after hornblende), opaque minerals (mostly Fe-Ti oxides) and accessory zircon.

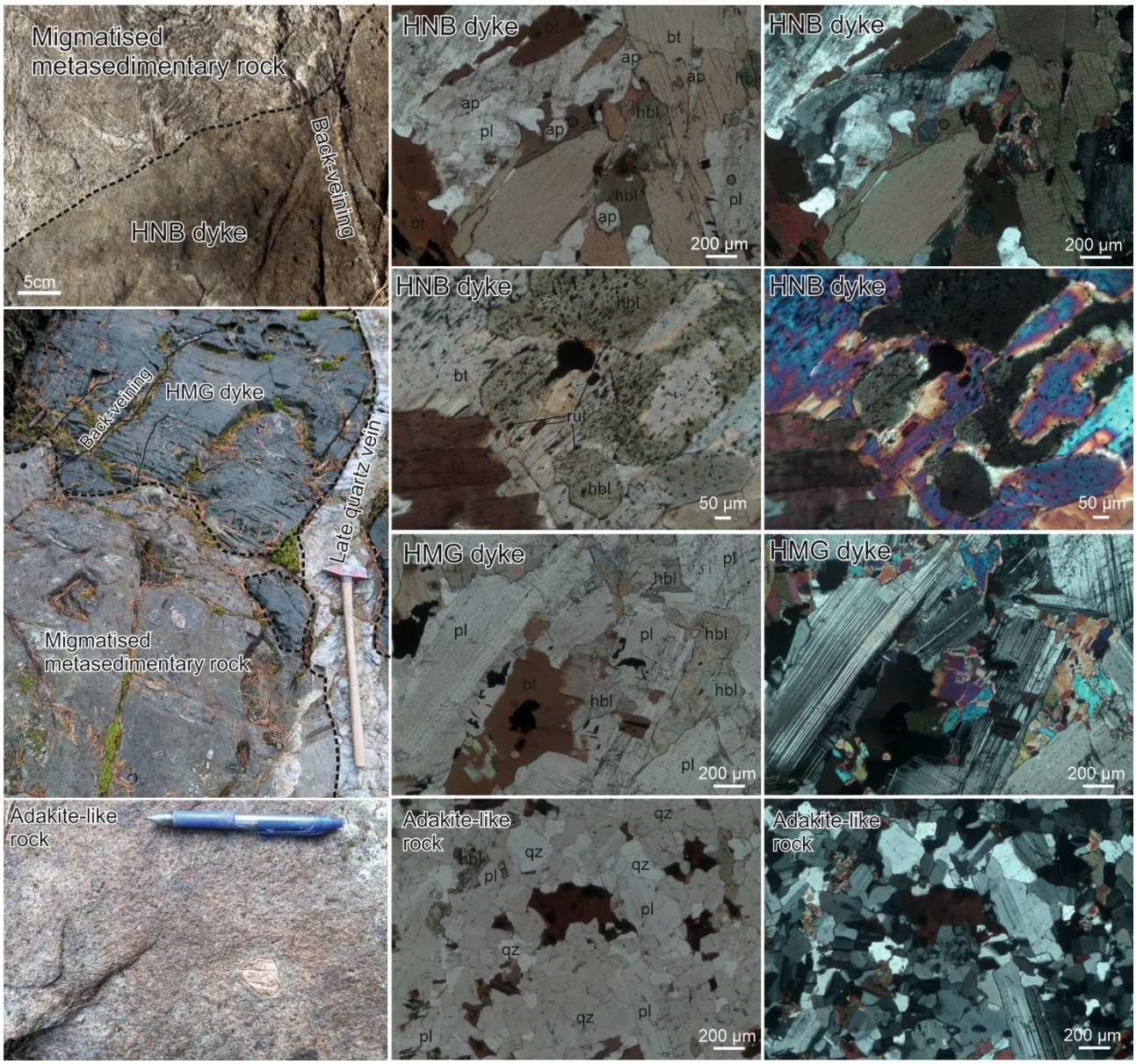


Fig. 3. Field examples (left column) and thin section photos (middle and right columns) of HNB, HMG and adakite-like rocks. A hammer (60 cm), a pen (15 cm) or a white bar for scale. Thin section photographs in the middle column in plane-polarized light and in the right column in cross-polarized light.

The HMG show $SiO_2$ contents between 45 and 54 wt.% and are classified as gabbros and gabbroic diorites in the total alkali vs. silica diagram (TAS; Fig. 4a). In the immobile trace element classification diagram (Fig. 4b), the samples form a rather tight cluster and are classified as basalts. The HMG exhibit MgO contents between 8 and 12 wt.% with one outlier at 17.7 wt.% MgO. $Na_2O$, $K_2O$ and $P_2O_5$ contents are low (<1.97 wt.%, <2.05 wt.% and <0.4 wt.%, respectively) but CaO contents are moderately high (>7.9 wt.%; Fig. 5). $Al_2O_3$ shows a large variation between 4.5 and 18 wt.%. The HMG are metaluminous and show high Mg-numbers between 56 and 70 (Fig. 5).

Kara, J., Väisänen, M., Heinonen, J. S., Lahaye, Y., O'Brien, H., & Huhma, H., 2020. Tracing arclogites in the Paleoproterozoic Era–A shift from 1.88 Ga calc-alkaline to 1.86 Ga high-Nb and adakite-like magmatism in central Fennoscandian Shield. Lithos, 372, 105663. https://doi.org/10.1016/j.lithos.2020.105663 (Author's postprint)

Table 1. Summary of the geochemistry, isotope data and modal compositions.

| | HMB (n=21) | | | HNB (n=14) | | | Adakite-like rocks (n=11) | | | GDGG (n=21) | | |
|---|---|---|---|---|---|---|---|---|---|---|---|---|
| | Avg | Max | Min | Avg | Max | Min | Avg | Max | Min | Avg | Max | Min |
| $SiO_2$ | 49.93 | 53.31 | 45.11 | 49.43 | 53.63 | 46.42 | 60.64 | 63.87 | 56.86 | 59.90 | 73.71 | 47.97 |
| $Al_2O_3$ | 13.82 | 17.26 | 4.42 | 15.43 | 16.85 | 11.33 | 16.22 | 17.10 | 15.64 | 15.86 | 18.38 | 13.39 |
| $Fe_2O_3^T$ | 10.96 | 15.11 | 8.67 | 12.39 | 15.42 | 10.98 | 6.92 | 8.49 | 4.92 | 7.71 | 11.81 | 2.06 |
| MgO | 10.32 | 17.74 | 8.02 | 5.19 | 11.67 | 3.79 | 3.25 | 4.49 | 1.86 | 3.38 | 7.07 | 0.44 |
| CaO | 10.05 | 12.52 | 7.95 | 7.02 | 8.37 | 6.20 | 4.98 | 6.25 | 3.87 | 5.10 | 10.34 | 0.24 |
| $Na_2O$ | 1.49 | 1.97 | 0.60 | 3.19 | 4.00 | 1.79 | 3.82 | 4.37 | 3.40 | 3.14 | 4.13 | 2.54 |
| $K_2O$ | 1.05 | 2.05 | 0.26 | 2.08 | 2.97 | 0.89 | 1.98 | 2.73 | 1.76 | 2.49 | 4.88 | 0.65 |
| $TiO_2$ | 0.95 | 1.46 | 0.46 | 2.06 | 2.91 | 1.66 | 0.88 | 1.12 | 0.54 | 0.81 | 1.62 | 0.16 |
| $P_2O_5$ | 0.13 | 0.36 | 0.05 | 0.83 | 1.16 | 0.67 | 0.22 | 0.29 | 0.14 | 0.16 | 0.34 | 0.03 |
| LOI | 1.25 | 2.20 | 0.20 | 1.31 | 2.30 | 0.60 | 0.74 | 1.30 | 0.40 | 1.11 | 1.90 | 0.50 |
| F | 440.00 | 863.00 | 108.00 | ###### | ###### | 994.00 | 511.36 | 676.00 | 358.00 | 515.06 | 859.00 | 157.00 |
| Ba | 160.71 | 253.00 | 66.00 | 655.33 | 768.00 | 412.00 | 542.73 | 897.00 | 428.00 | 488.00 | 990.00 | 134.00 |
| Rb | 42.56 | 106.60 | 7.40 | 61.19 | 133.60 | 25.30 | 58.99 | 84.30 | 48.00 | 92.09 | 183.20 | 14.70 |
| Sr | 233.44 | 403.80 | 86.30 | 937.55 | 1521.20 | 445.10 | 547.69 | 637.20 | 399.00 | 307.07 | 544.30 | 89.70 |
| Zr | 62.46 | 111.00 | 24.60 | 280.98 | 404.90 | 194.50 | 158.28 | 239.40 | 121.20 | 181.14 | 524.80 | 75.90 |
| Hf | 1.87 | 3.00 | 1.10 | 6.23 | 9.20 | 4.20 | 3.97 | 5.90 | 3.00 | 4.94 | 12.80 | 2.20 |
| Nb | 5.79 | 10.50 | 1.70 | 34.92 | 44.00 | 18.90 | 12.78 | 17.50 | 10.70 | 10.93 | 22.50 | 4.90 |
| Ta | 0.50 | 1.50 | 0.20 | 1.48 | 2.30 | 1.00 | 0.76 | 1.00 | 0.60 | 0.78 | 1.50 | 0.30 |
| Y | 18.76 | 23.90 | 10.80 | 30.18 | 47.90 | 22.20 | 13.68 | 17.20 | 10.30 | 20.94 | 34.90 | 7.80 |
| Th | 1.45 | 3.10 | 0.30 | 3.69 | 6.50 | 1.50 | 5.37 | 8.80 | 3.90 | 7.28 | 18.40 | 0.90 |
| U | 0.86 | 2.60 | 0.20 | 1.95 | 2.70 | 1.00 | 2.15 | 3.60 | 1.30 | 2.49 | 4.70 | 0.90 |
| Cr | 635.12 | 978.45 | 266.85 | 110.05 | 561.07 | 13.68 | 62.20 | 109.48 | 20.53 | 69.40 | 191.58 | 13.68 |
| Ni | 51.13 | 107.60 | 6.80 | 32.50 | 200.50 | 4.40 | 29.15 | 49.00 | 13.40 | 17.52 | 72.20 | 1.80 |
| Pb | 19.71 | 140.50 | 1.90 | 3.89 | 5.00 | 2.50 | 7.26 | 22.20 | 2.30 | 3.58 | 5.80 | 0.80 |
| La | 10.41 | 20.00 | 5.10 | 57.33 | 70.30 | 29.60 | 23.27 | 32.00 | 12.40 | 29.11 | 51.40 | 8.00 |
| Ce | 25.64 | 51.00 | 10.80 | 132.00 | 182.40 | 80.50 | 47.57 | 66.90 | 25.70 | 61.46 | 117.70 | 20.80 |
| Nd | 15.19 | 32.20 | 7.10 | 69.61 | 104.50 | 50.60 | 20.92 | 30.00 | 12.30 | 26.96 | 48.20 | 13.40 |
| Sm | 3.53 | 6.36 | 1.95 | 12.11 | 19.83 | 9.70 | 4.07 | 5.69 | 2.99 | 5.37 | 10.05 | 3.32 |
| Eu | 1.05 | 1.83 | 0.45 | 3.02 | 4.55 | 2.30 | 1.16 | 1.42 | 0.89 | 1.17 | 2.22 | 0.52 |
| Gd | 3.65 | 5.48 | 2.00 | 9.55 | 15.33 | 7.81 | 3.46 | 4.35 | 2.68 | 4.72 | 8.19 | 2.92 |
| Tb | 0.58 | 0.79 | 0.34 | 1.20 | 1.97 | 0.94 | 0.48 | 0.60 | 0.39 | 0.69 | 1.16 | 0.42 |
| Dy | 3.49 | 4.55 | 1.95 | 6.21 | 10.30 | 4.67 | 2.65 | 3.47 | 2.05 | 3.89 | 6.42 | 1.97 |
| Ho | 0.71 | 0.88 | 0.42 | 1.12 | 1.81 | 0.81 | 0.51 | 0.64 | 0.40 | 0.78 | 1.31 | 0.29 |
| Yb | 1.94 | 2.50 | 1.10 | 2.63 | 4.11 | 1.93 | 1.29 | 1.77 | 1.02 | 2.04 | 3.40 | 0.71 |
| Lu | 0.29 | 0.39 | 0.16 | 0.38 | 0.57 | 0.27 | 0.19 | 0.27 | 0.15 | 0.31 | 0.51 | 0.11 |
| Fe/Mn | 58.08 | 70.30 | 46.80 | 67.64 | 71.90 | 62.70 | 71.74 | 88.80 | 63.40 | 67.18 | 95.70 | 46.50 |
| $(La/Yb)_{CN}$ | 3.90 | 6.48 | 1.90 | 14.33 | 24.31 | 7.24 | 11.97 | 14.74 | 8.09 | 9.01 | 47.00 | 2.53 |
| $(La/Sm)_{CN}$ | 1.86 | 2.42 | 0.85 | 2.86 | 3.73 | 1.90 | 3.55 | 4.71 | 2.75 | 2.64 | 5.66 | 1.30 |
| $(Dy/Yb)_{CN}$ | 1.21 | 1.56 | 1.01 | 1.55 | 1.77 | 1.44 | 1.34 | 1.56 | 1.15 | 1.29 | 2.13 | 1.05 |
| Eu/Eu* | 0.88 | 1.17 | 0.60 | 0.88 | 1.03 | 0.65 | 0.96 | 1.12 | 0.84 | 0.81 | 1.09 | 0.58 |
| Ce/Ce* | 1.02 | 1.10 | 0.93 | 1.02 | 1.07 | 0.97 | 1.02 | 1.16 | 0.94 | 1.00 | 1.17 | 0.90 |
| WR eNd | | +3.8 | | | +2.4 | | | +3.1 | | | +2.8 (granodiorite) | |
| Zircon eHf[1] | +3.3 | -0.4 | +9.4 | -2.0 | +6.5 | -8.8 | -4.0 | +0.3 | -12.6 | -2.8/-0.8 | -7.1/-3.8 | +0.5/+4.8 |
| crystallisation age | | 1.86 Ga | | | 1.86 Ga | | | 1.86 Ga | | | 1.88 Ga | |
| Na-pl | | - | | | - | | | ++ | | | n.a. | |
| Ca-pl | | ++ | | | ++ | | | - | | | n.a. | |
| hbl | | ++ | | | ++ | | | + | | | n.a. | |
| qz | | - | | | - | | | ++ | | | n.a. | |
| bt | | + | | | ++ | | | + | | | n.a. | |
| opx | | - | | | - | | | +/- | | | n.a. | |
| kfs | | - | | | - | | | +/- | | | n.a. | |
| zr | | + | | | + | | | + | | | n.a. | |
| mz | | - | | | + | | | - | | | n.a. | |
| rt | | - | | | + | | | - | | | n.a. | |
| ap | | - | | | + | | | - | | | n.a. | |
| ttn | | +/- | | | +/- | | | +/- | | | n.a. | |
| bd | | - | | | + | | | - | | | n.a. | |

[1] HMB: only 10-MJV-02 included; HNB: 033.1- and 033.3-JKA-015 combined; GDGG: gabbro (024-JKA-015)/granodiorite (136.1-JKA-015) CN=Chondrite normalized; WR=whole rock; pl=plagioclase; hbl=hornblende; qz=quartz; bt=biotite; opx=orthopyroxene; kfs=K-feldspar; zr=zircon; mz=monazite; rt=rutile; ap=apatite; ttn=titanite; bd=baddeleyite; ++=abundant; +=present; +/-=possibly present; -=not detected; n.a.=not analysed

The HMG generally show low trace element contents but the internal variation within the group is large. All the samples are enriched in Cr and are also enriched in Ni (Fig. 6). In the multielement diagram, the HMG show depletion in Nb, Ta, P, Zr, Hf and Ti but enrichment in Rb, Ba, Pb and LREE (Fig. 7a). The HMG show moderate but variably fractionated REE patterns (Fig. 7b) where $(La/Yb)_{CN}$ = 1.9–7.1 (Table 1).

### *4.1.3. High-Nb gabbros*

The HNB show similar field relations as the HMG. The HNB exhibit granular to subophitic texture with primary hornblende and biotite surrounded by abundant Ca-plagioclase (Fig. 3). Apatite occurs as large (up to 2 mm) crystals. Accessory phases include zircon, monazite, titanite, rutile and opaques (Fe-Ti oxides).

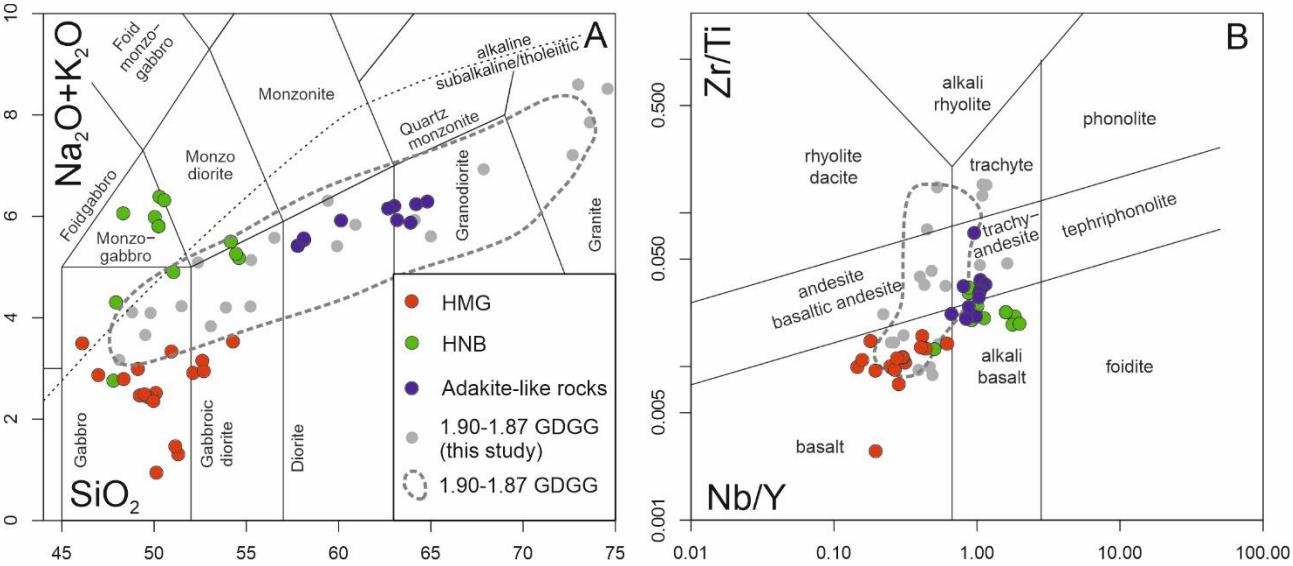


Fig. 4. A) Total alkali vs. silica (TAS) diagram (Middlemost, 1994; division between tholeiitic and alkaline rock series after Le Bas et al., 1984) and B) Zr/Ti vs. Nb/Y classification diagram (Winchester & Floyd, 1977). 1.90–1.87 Ga calc-alkaline gabbro-diorite-granodiorite-granite (GDGG) series with arc affinities, including their volcanic counterparts, shown for comparison (grey dots = this study; dashed field = samples after Hakkarainen, 1994 and Lahtinen, 1996).

The HNB show $SiO_2$ contents between 47 and 54 wt.% and are classified mostly as monzogabbros and monzodiorites with three samples plotting as gabbros and two as gabbroic-diorites (Fig. 4a). The total alkali contents are > 4 wt.% apart from one gabbroic outlier (031.1-JKA-015) with a total alkali content of 2.5 wt.%. In the immobile trace element classification diagram (Fig. 4b), the samples plot in two separate groups, one each in the alkali basalt and trachyandesite fields with one basaltic outlier (031.1-JKA-015). The HNB show high $Fe_2O_3^T$ (> 11.0 wt.%), $TiO_2$ (> 1.7 wt.%) and $P_2O_5$ (> 0.7 wt.%), but low to moderate MgO and CaO contents. Mg-numbers are low except for one outlier with high MgO content (031.1-JKA-015). The HNB are metaluminous (Fig. 5).

The HNB show high HFSE contents, especially in Nb (18.9–44 ppm), which is one characteristic features of this group. The HNB are also enriched in LREE, F and certain LILE such as Ba and Sr. The HNB show low concentrations of Cr and Ni except for gabbroic sample 031.1-JKA-015 (Fig. 6). In the multielement diagram (Fig. 7a), the group shows slight internal variation in Nb-Ta and Zr-Hf enrichment levels: the HNB mostly lack clear Nb (Nb/Nb* = 0.45–1.48) and Zr-Hf troughs although they are visible in some sample profiles. The HNB show high concentrations of REE ($\sum_{REE}$ = 204–443 ppm) and the REE pattern is highly fractionated (Fig. 7b) with $(La/Yb)_{CN}$ = 9.2–24.3. A small negative Eu anomaly is visible in some HNB REE profiles (Table 1; Fig. 7b).

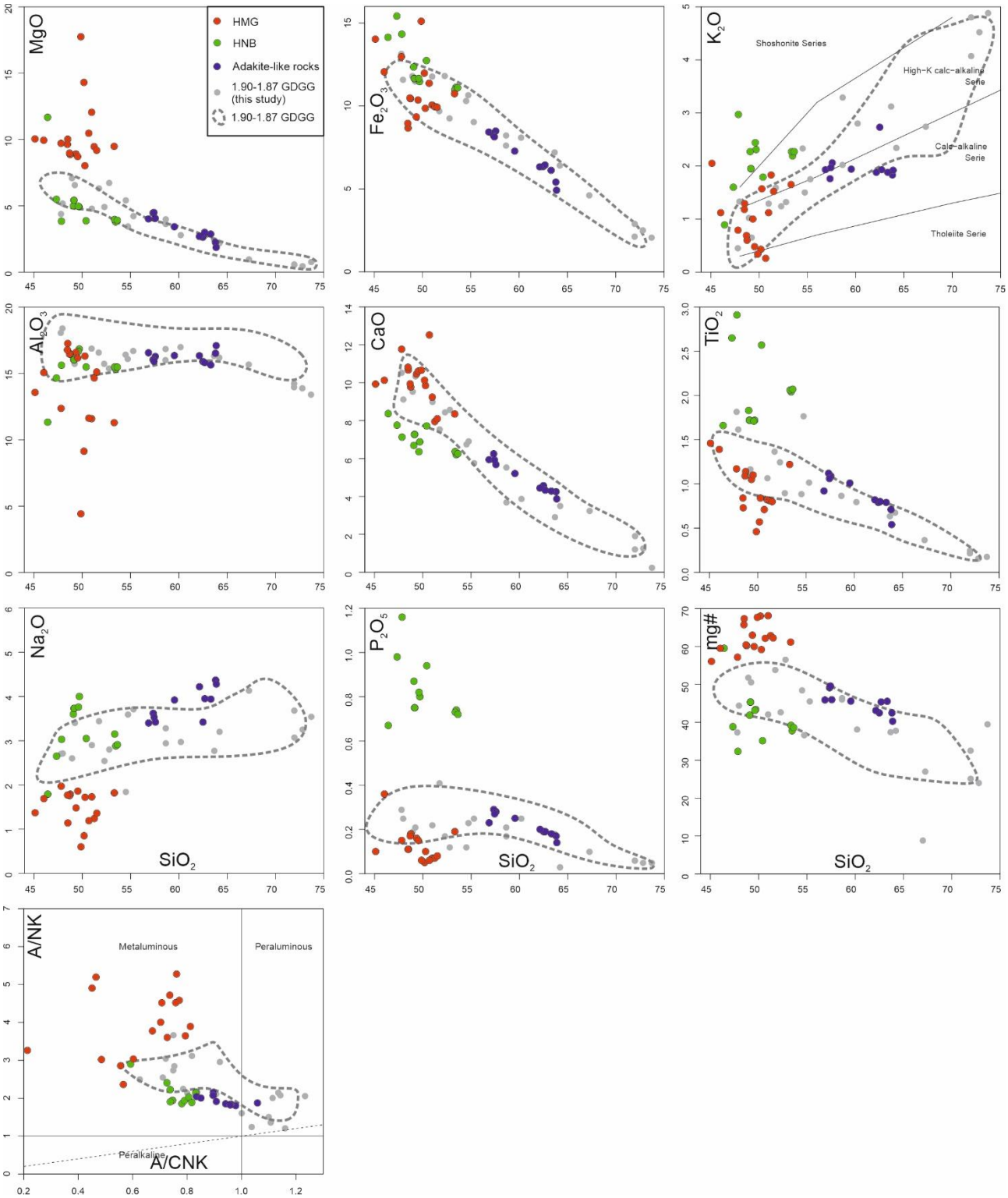


Fig. 5. Major element (wt.%) vs. SiO2 (wt.%) diagrams. Mg-number (mg# = MgO/(FeO + MgO) [mol. %]) calculated with GCDKit software (Janousek et al., 2006). Alumina saturation diagram A/CNK vs. A/NK is after Shand (1943).

### *4.1.4. Adakite-like rocks*

Adakite-like rocks show geochemical features similar to adakites (Martin et al., 2005) but the "adakitic" signature is not particularly strong. Based on field observations, the group includes intermediate plagioclase- and hornblende-phyric dykes and small tonalite and quartz diorite intrusions. The dykes display a porphyritic texture with Na-plagioclase and hornblende phenocrysts in a matrix of Na-plagioclase, quartz, biotite and hornblende. Accessory phases include apatite and

zircon. The tonalites have similar modal composition but exhibit equigranular textures. The quartz diorites have accessory quartz and contain more hornblende and opaque minerals than the tonalites.

The adakite-like rocks show a range of $SiO_2$ contents between 57 and 64 wt. % and are classified as diorites and granodiorites in the TAS diagram (Fig. 4a). The samples form a coherent group in the trace element classification diagram straddling the alkali basalt and trachyandesite fields with one outlier near the trachyte field (Fig. 4b). The $Al_2O_3$ and $Na_2O$ contents are high (>15.5 wt. %, >2.9 wt. %, respectively), MgO content is moderate between 1.9 and 4.5 wt. %, but $K_2O$, $Fe_2O_3^T$ and $P_2O_5$ contents are rather low (Fig. 5). The group shows slight depletion of MgO, $Fe_2O_3^T$, CaO, $TiO_2$ and $P_2O_5$ with increasing silica content. The Mg-numbers are between 40 and 50 and the samples can be classified as metaluminous with one peraluminious outlier (Fig. 5).

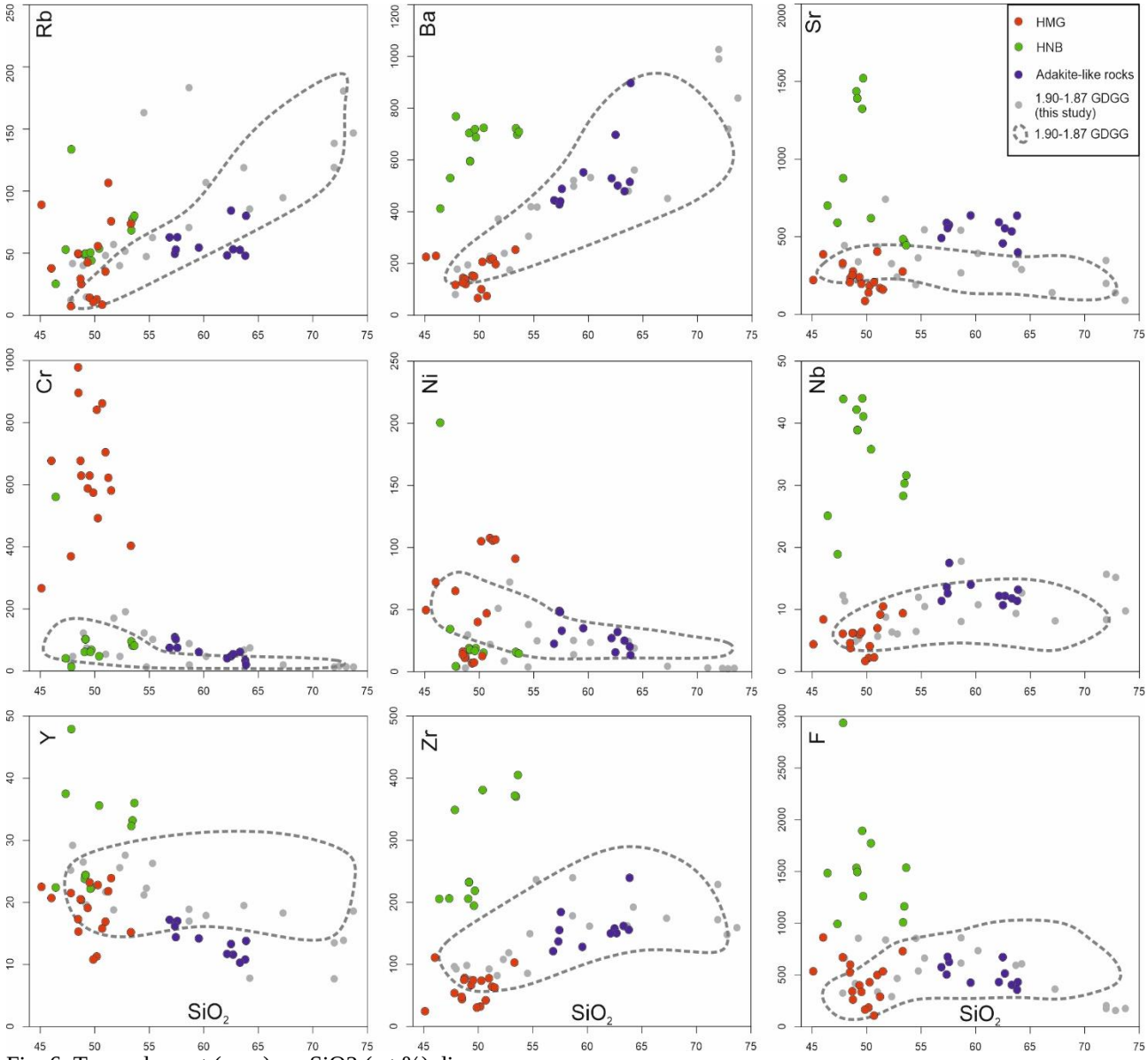


Fig. 6. Trace element (ppm) vs. SiO2 (wt.%) diagrams.

The adakite-like rocks are enriched in most LILE, especially in Sr (>400 ppm; Fig. 6). They show moderate Zr, Nb, Ni and Cr concentrations but are depleted in Y (<18 ppm; Fig. 6). In the multielement diagram the samples are enriched in LILE, Th and Pb but depleted in Nb, Ta, P and Ti

(Fig. 7a). The REE pattern is steep ($(La/Yb)_{CN}$ = 8.1–14.7) with high LREE concentrations and low HREE concentrations (Fig. 7b).

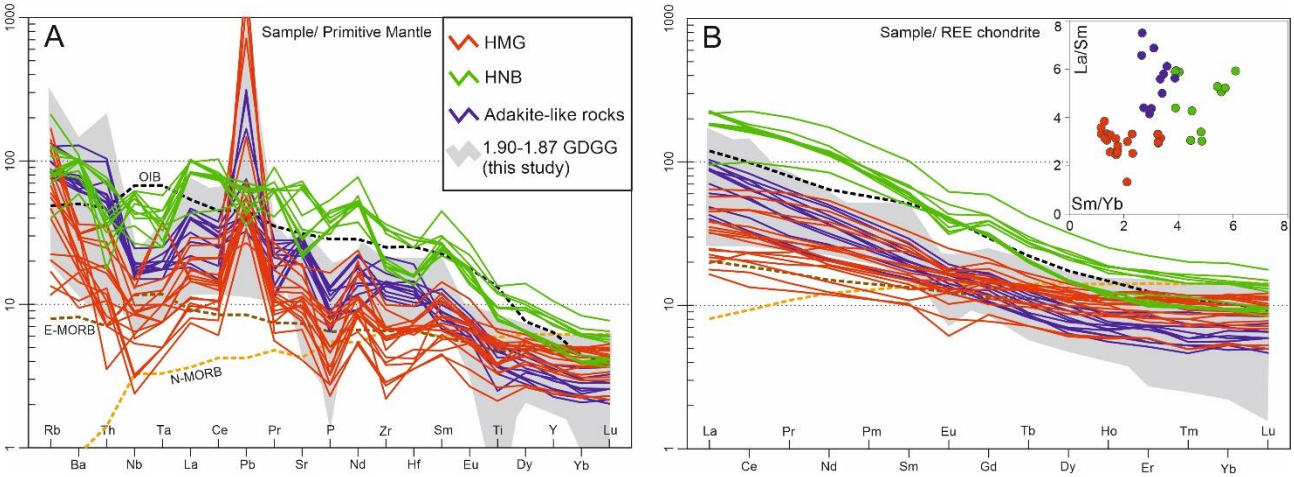


Fig. 7. Multielement diagrams normalized to primitive mantle (A; Sun and McDonough, 1989) and REE diagram normalized to C1 chondrite (B; Boynton, 1984). OIB, E-MORB and N-MORB reference patterns after Sun & McDonough (1989). La/Sm vs. Sm/Yb diagram shown as inset in B.

### *4.2. U-Pb age data*

The U-Pb data tables can be found in Electronic Appendix C and detailed U-Pb data interpretation can be found in Electronic Appendix D. The obtained magmatic ages are concentrated into two major groups: 1880 and 1860 Ma.

From the total of seven dated samples, two belong to the HMG group; 10-MJV-02 is from an approximately 1000 m long and 50 m wide medium-grained gabbro dyke and 085.1-JKA-015 is from a narrow, approximately 50 cm wide, fine-grained gabbro dyke. Two samples are from the HNB group; 033.1-JKA-015 and 033.3-JKA-015 represent coarse- and fine-grained varieties of the same or adjacent monzogabbro intrusion(s). Sample 026.1-JKA-015 is from a plagioclase- and hornblende-phyric dyke and belongs to the adakite-like rock group. In addition, two samples from the GDGG group were analysed; 024.1-JKA-015 is a medium-grained gabbro and 136.1-JKA-015 is a medium-grained granodiorite. A few monazites were recovered from the two HNB samples mentioned above and a pooled U-Pb monazite age was calculated due to scarcity of data.

#### *4.2.1. Gabbro-diorite-granodiorite-granite series*

The gabbro sample 024.1-JKA-015 contains two texturally distinct zircon groups (Fig. 8a): one with large elongated crystals (length up to 500µm, width-length 1:3) and the other with rounded, smaller grains (50–150 µm length, 50–100 µm width). All the zircons are quite homogeneous, but especially the larger variety shows cores and inner domains with abudant cracks. In total, 58 analyses were performed on 46 grains of which 21 analyses yield a concordia age of 1880 ± 5 Ma (2σ; MSWD = 0.68; Fig. 9a). Most of the analyses have suffered Pb loss (n = 24) and they were rejected from the concordia age calculation. If these analyses are included, a $^{207}Pb/^{206}Pb$ age of 1878 ± 3 Ma (2σ; MSWD = 0.28; not shown) and an upper intercept age of 1877 ± 4 Ma (2σ; MSWD = 0.30; not shown) can be obtained. Eight analyses show older $^{207}Pb/^{206}Pb$ ages between 1900 and 1921 Ma and five analyses younger $^{207}Pb/^{206}Pb$ ages between 1867 and 1836 Ma.

The zircons from the granodiorite sample 136.1-JKA-015 are homogeneous, rounded and typically elongated (50–200 µm in length and having width-length ratios of 1:2; Fig. 8b). The grains mostly lack internal structures, but a few cores can be found. Thirty-one analyses out of 76 (65 grains) yield a concordia age of 1881 ± 4 Ma (2σ; MSWD = 2.3; Fig. 9b). Five analyses were rejected due to

Kara, J., Väisänen, M., Heinonen, J. S., Lahaye, Y., O'Brien, H., & Huhma, H., 2020. Tracing arclogites in the Paleoproterozoic Era–A shift from 1.88 Ga calc-alkaline to 1.86 Ga high-Nb and adakite-like magmatism in central Fennoscandian Shield. Lithos, 372, 105663. https://doi.org/10.1016/j.lithos.2020.105663 (Author's postprint)

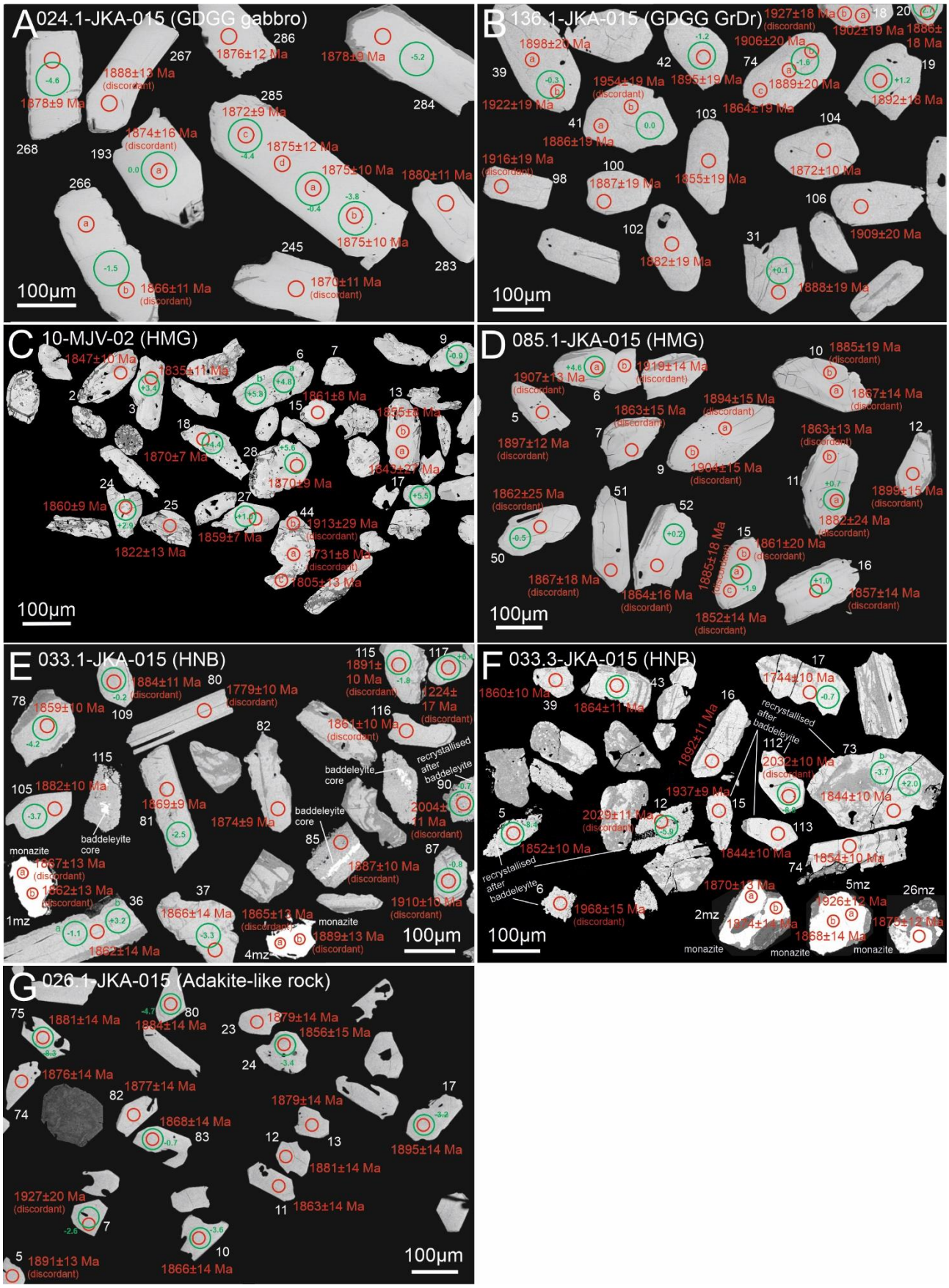


Fig. 8. Representative BSE-images of the analysed zircons and monazites. Sample names, rock groups, 207Pb/206Pb ages (in red, smaller spot) and initial $\varepsilon_{Hf}$ values (in green, larger spot) indicated.

discordance but a $^{207}Pb/^{206}Pb$ age of 1882 ± 4 Ma (2σ; MSWD = 0.32; not shown) and an upper intercept age of 1880 ± 5 Ma (2σ; MSWD = 0.28; not shown) are calculated if these analyses are included. The rest of the analyses yield older $^{207}Pb/^{206}Pb$ ages between 1970 and 1895 Ma (n = 34) or younger $^{207}Pb/^{206}Pb$ ages between 1868 and 1848 Ma (n = 6). Eight analyses were rejected due to high common Pb.

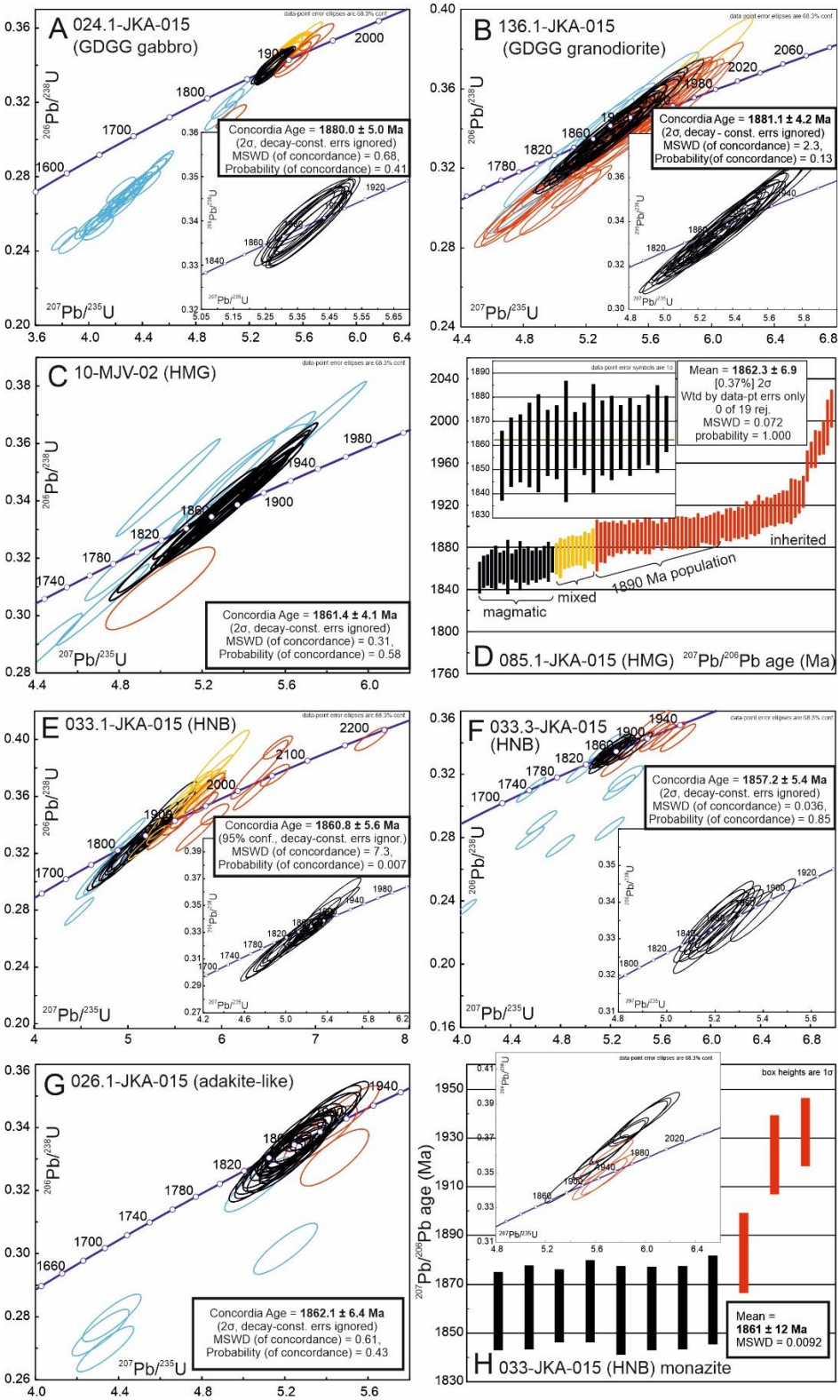


Fig. 9. U-Pb data for the analysed zircons and monazites. Black = age of magmatism; red = inherited grain or older age; yellow = mixed or reversely concordant age; blue = Pb loss, discordance or young age.

#### *4.2.2. High-Mg gabbros*

Sample 10-MJV-02 shows a wide range of zircon shapes (Fig. 8c). The grains are mostly elongated, 50–300 µm in length and 10–200 µm in width. They are anhedral and rounded and contain abudant inclusions, resorption features and domains with varied textures. Cores or core-like structures, overgrowths and rims of varying thicknesses can be found. Most of the grains show faint growth zonation. Metamictization is common and has developed preferentially between contrasting textural domains. In total, 27 spots were analysed on 24 grains. Ten analyses were rejected due to high common Pb or high discordance. The remaining 17 analyses yield a concordia age of 1861 ± 4 Ma (2σ; MSWD = 0.31; Fig. 9c).

Sample 085.1-JKA-015 shows three kinds of zircon shapes (Fig. 8d): 1) fragments from bigger zircons with width-length ratios of 1:2; 2) rounded and rather small grains with width-length ratios of 1:1.5; and 3) elongated grains of which most show growth zoning and width-length ratios of 1:4. The grain textures in all groups are more homogeneous compared to sample 10-MJV-02. However, cores and thin rims are common. In total, 85 analyses were performed on 70 grains but most of the grains have suffered major Pb loss and therefore no concordia age was calculated. Nineteen analyses yield a $^{207}Pb/^{206}Pb$ age of 1862 ± 7 Ma (2σ; MSWD = 0.072; Fig. 9d) and an upper intercept age of 1864 ± 12 Ma (95 %; MSWD = 0.075; not shown). Most analyses (n = 56) show older $^{207}Pb/^{206}Pb$ ages between 2012 and 1882 Ma and ten analyses are apparently mixed between the crystallisation age and the older ages. From the older population a cluster of 31 zircons with an age of approximately 1890 Ma can be distinguished. The crystal habit of zircon largely correlates with age so that most of the elongated and rounded grains belong to the 1860 Ma population while the fragmentary grains have older ages. Seven analyses were rejected from the age calculations due to high common Pb.

#### *4.2.3. High-Nb gabbros*

Samples 033.1-JKA-015 and 033.3-JKA-015 show similar zircon shapes (Fig. 8e, f). The grains are heterogeneous but two main groups can be distinguished: 1) sponge-like, porous, resorbed and very rounded grains and 2) angular grains. The grains from the spongy group are only slightly elongated with lengths between 50–150 µm and width-length ratios of 1:1.5–2. Some grains from this group contain baddeleyite cores. The angular grains are usually variably metamict. About half of the angular grains show growth zoning and the rest seem to lack a clear internal structure. Only a few cores can be identified, but some grains have small inclusions of baddeleyite or monazite (Fig. 8e, f). In total, 56 analyses were performed on 54 grains for 033.1-JKA-015. Twenty-one analyses, including two analyses from the spongy group, yield a concordia age of 1861 ± 6 Ma (2σ; MSWD = 7.3; Fig. 9e). A similar $^{207}Pb/^{206}Pb$ age of 1863 ± 5 Ma (2σ; MSWD = 0.48; not shown) and an upper intercept age of 1861 ± 5 (MSWD = 0.75; plot not shown) are obtained when the discordant analyses are included (n=31). Fourteen analyses, including nine analyses from the spongy group, show older $^{207}Pb/^{206}Pb$ ages between 2196 and 1878 Ma. Two younger analyses with $^{207}Pb/^{206}Pb$ ages of 1848 and 1779 Ma were also determined. The rest of the analyses were rejected due to high common Pb or high discordance. For sample 033.3-JKA-015, 31 analyses were performed on 31 grains. Twelve analyses yield a concordia age of 1857 ± 5 Ma (2σ; MSWD = 0.036; Fig. 9f) and 15 analyses show a $^{207}Pb/^{206}Pb$ age of 1860 ± 9 Ma (95 %; MSWD = 2.2; not shown) including seven analyses on spongy zircons. Three analyses show younger $^{207}Pb/^{206}Pb$ ages between 1828 and 1744 Ma. Twelve analyses were rejected due to high common Pb or high discordance.

The monazites from both samples are rounded, 70–200 µm in both length and width and usually show outer growths of other minerals, such as zircon or titanite (Fig. 8 e, f). Eight analyses out of 11 yield a weighted average age of 1861 ± 12 Ma (2σ; MSWD = 0.0092). Three analyses show older $^{207}Pb/^{206}Pb$ ages between 1933 and 1883 Ma (Fig. 9h).

#### *4.2.4. Adakite-like rocks*

The droplet-like zircons from 026.1-JKA-015 are rather small, slightly elongated and homogeneous (Fig. 8g). The grains are about 100 µm in length and 70 µm in width. They do not show clear zoning or other internal structures. A total of 33 analyses were performed on 33 grains. Six analyses were rejected from the concordia age calculation due to a high discordance or common Pb and two analyses due to older ages ($^{207}Pb/^{206}Pb$ ages of 1885 and 1888 Ma). The remaining 25 analyses yield a concordia age of 1862 ± 6 Ma (2σ; MSWD = 0.61; Fig. 9g).

### *4.3. Sm-Nd isotope data*

The whole rock Sm-Nd isotopes were analysed from one sample in each group. The data are available in Electronic Appendix B and illustrated in Fig. 10. All the initial $\varepsilon_{Nd}$ values are depleted relative to CHUR and plot on or slightly below depleted mantle compositions (Fig. 10). The most depleted Nd isotopic composition is recorded by the HMG sample 10-MJV-02 (initial $\varepsilon_{Nd}$ = +3.8 at 1860 Ma; $T_{DM}$ = 1865 Ma) and the most enriched composition by the HNB sample 033.3-JKA-015 (initial $\varepsilon_{Nd}$ = +2.4 at 1860 Ma; $T_{DM}$ = 1954 Ma). The adakite-like sample 026.1-JKA-015 (initial $\varepsilon_{Nd}$ = +3.1 at 1860 Ma; $T_{DM}$ = 1914 Ma) and the GDGG sample 182.1-JKA-015 (same rock unit as 136.1-JKA-015 that was analysed for U-Pb-Hf isotopes in zircon; initial $\varepsilon_{Nd}$ = +2.8 at 1880 Ma; $T_{DM}$ = 1951 Ma) plot intermediate to the HMG and HNB samples.

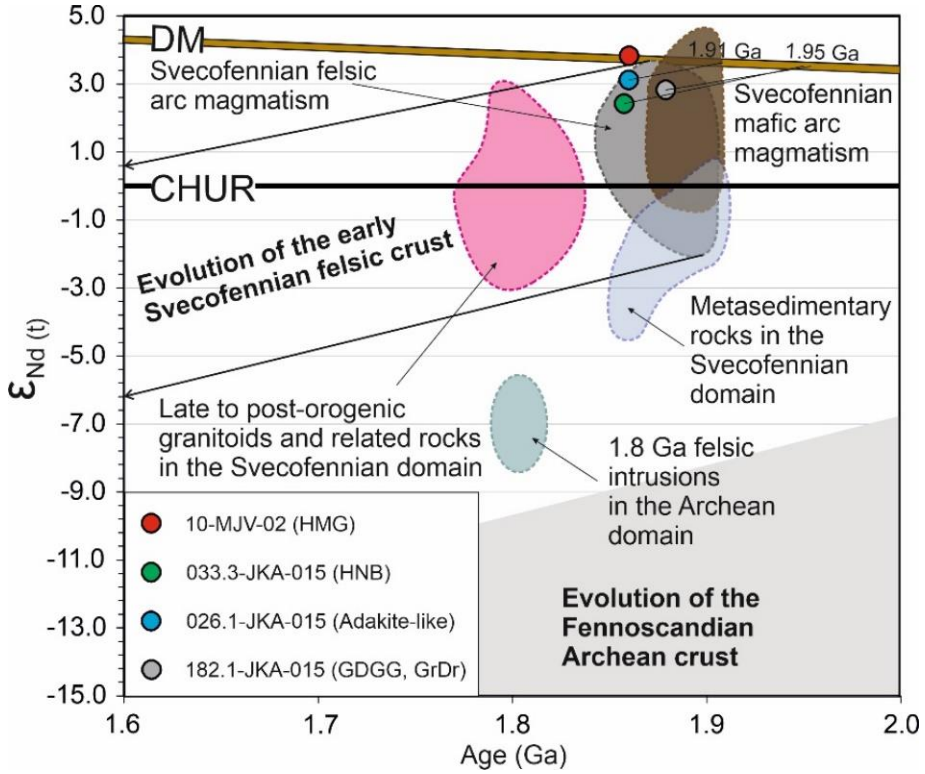


Fig. 10. $\varepsilon_{Nd}$ (t) vs. Age (Ga) diagram showing data from this study and relevant reference data and evolution trends of the Svecofennian bedrock. Modified after compilation by Kara et al. (2018) and references therein.

### *4.4. Zircon Lu-Hf isotope data*

The zircon Lu-Hf isotope data are available in Electronic Appendix E and illustrated in Fig. 11. In general, the zircon Hf isotopic compositions show a high degree of variability from depleted mantle –like values recorded by some zircons in HMG sample 10-MJV-02 to considerably enriched values recorded by adakite-like sample 026.1-JKA-015. Within-sample variation is also large with ranges spanning from 8 to up to 13 $\varepsilon_{Hf}$ units. The results are described in detail below.

All the analyses (n=21) of sample 024.1-JKA-015 (GDGG, gabbro) were from the 1880 Ma zircon population and they show variation in initial $\varepsilon_{Hf}$ values between -7.1 and +0.5 with an average value of -2.8. Twenty-two spots analysed on zircons from sample 136.1-JKA-015 (GDGG, granodiorite) show initial $\varepsilon_{Hf}$ values between -3.8 and +4.8 with an average value of -0.8 (at 1880 Ma). The six analyses on inherited zircons show variation in initial $\varepsilon_{Hf}$ values between -10.9 and +1.9 with age varying from 1912 to 1936 Ma.

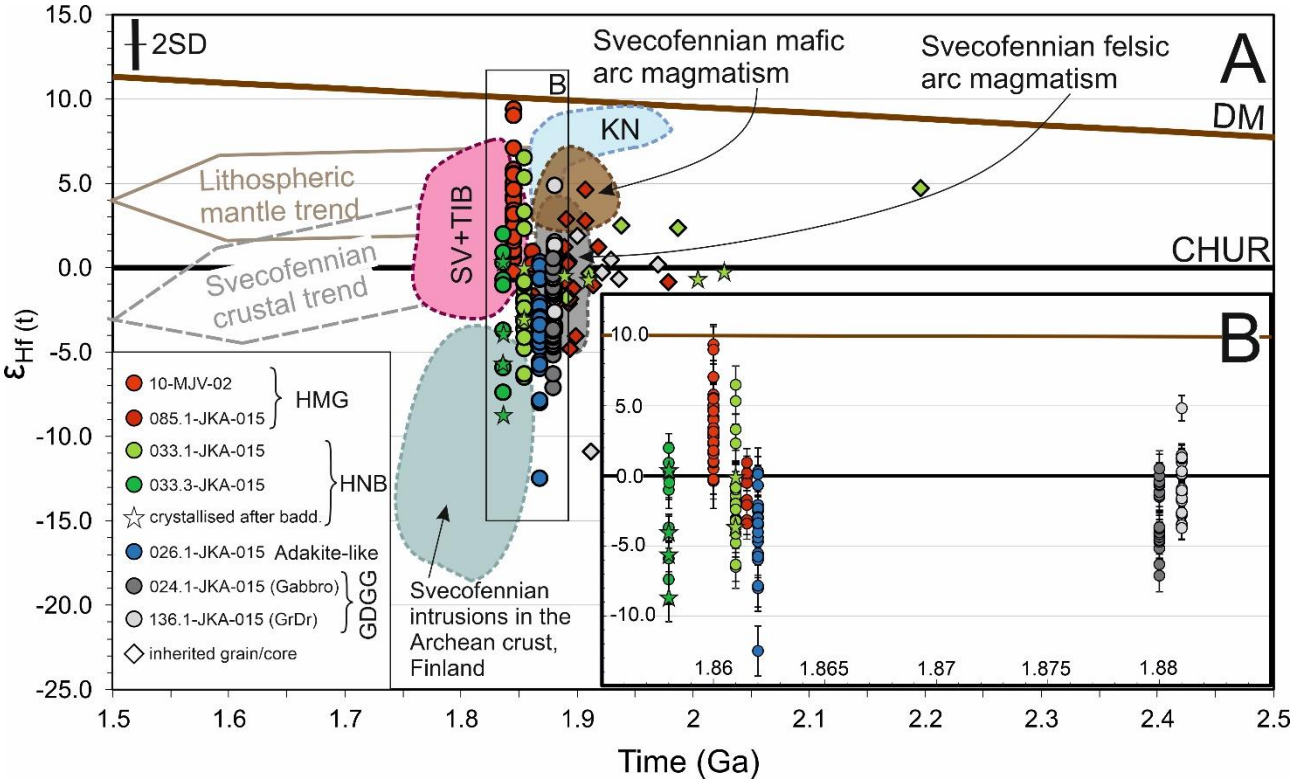


Fig. 11. εHf (t) vs. Age (Ga) diagram showing data from this study (A and B) and relevant reference data from the Svecofennian bedrock (only A).Modified after compilation by Kara et al. (2018) and references therein. KN = Knaften arc, SV+TIB = Syn to late orogenic Svecofennian and Transcandinavian Igneous Belt granitoids.

In total, 36 analyses were performed on sample 10-MJV-02 (HMG). They show variation in initial $\varepsilon_{Hf}$ values between -0.4 and +9.4 with an average value of +3.3 at 1860 Ma. The 1860 Ma zircon population (n=8) from sample 085.1-JKA-015 (HMG) yielded initial $\varepsilon_{Hf}$ values between -3.4 and +1.0 with an average value of -1.2. The inherited zircons from the same sample exhibit variation in initial $\varepsilon_{Hf}$ values between -4.8 and +4.6 with age varying from 1893 to 1979 Ma.

Twenty-four analyses were performed on the 1860 Ma population on sample 033.1-JKA-015 (HNB). They exhibit variation in initial $\varepsilon_{Hf}$ values between -6.5 and +6.5 with an average value of -1.6 including two analyses on the spongy zircons. Nine inherited zircons, including four analyses on the spongy zircons, exhibit variation in initial $\varepsilon_{Hf}$ values between -1.8 and +4.7 with age varying from 2196 to 1889 Ma. A total of 12 analyses were performed on sample 033.3-JKA-015 (HNB) including four analyses on the spongy zircons. They show variation in initial $\varepsilon_{Hf}$ values between -8.4 and +2 with an average value of -2.8 at 1860 Ma.

A total of 23 analyses were performed on sample 026.1-JKA-015 (adakite-like rock). They show variation in initial $\varepsilon_{Hf}$ values between -12.6 and 0.3 with an average value of -4.0 at 1860 Ma.

## 5. Discussion

### *5.1. Age constraints and relationships of zircon and baddeleyite*

Subduction-related arc magmatism started at 1.90 Ga in southern Central Svecofennia, which is recorded by calc-alkaline volcanism in the Tampere belt (Kähkönen, 1989; Lahtinen, 1996; Kähkönen, 2005) and continued until 1.87 Ga in the Pirkanmaa belt and in whole Southern Svecofennia (Kähkönen, 2005; Nironen, 2005 and references therein; Kara et al., 2018). Also, the two GDGG samples in this study show a precise concordia age of 1880 Ma which is considered as a crystallisation age for both samples (Fig. 9a and b; Electronic Appendix D). The HMG, HNB and adakite-like groups clearly show younger crystallisation ages around 1860 Ma (Fig. 9c, d, e, f, g and h; Electronic Appendix D). The change in the nature and volume from the well-recorded synorogenic ~1.88 Ga magmatism to the sporadic ~1.86 Ga magmatism is clear. In fact, in Central Svecofennia and the Central Finland Granitoid Complex there is only one example of a 1.86 Ga intrusion (Halkoaho et al., 2020) and Kukkonen et al. (2008) argued that homogenous warming of the lithosphere led to cessation of magmatic activity after 1.875 Ga. In Southern Svecofennia, a few intraorogenic mafic intrusions (Väisänen et al., 2012a, 2012b; Nevalainen et al., 2016) seem to share similar geochemical features with each other and thus a similar geodynamic environment. The decrease in the magmatic activity might be due to several reasons. Thickening and warming of the lithosphere (Kukkonen et al., 2008; Lahtinen et al., 2009a) as well as the end of the subduction (Lahtinen, 2005; Hermansson et al., 2008) are probably the main factors.

Inherited zircons are common in all the 1.86 Ga samples, except in HMG sample 10-MJV-02. These ages span 2196–1870 Ma and are similar to ages of detrital grains found in the Svecofennian metasedimentary rocks suggesting some interaction of the magmas with such crustal wallrocks (e.g., Huhma et al., 1991; Lahtinen et al., 2009b). Another possible source for the zircons is the GDGG rocks. For example, in the adakite-like sample 026.1-JKA-015, two inherited grains were found with ages around 1885 Ma corresponding to those reported for the magmatic zircons in the GDGG rocks. Interestingly, all the zircons in the adakite-like sample show uniform Th/U and morphology indicating that the zircons derive from a uniform source. Inherited grains (1970–1895 Ma) having likely sources in the Svecofennian metasedimentary rocks are also found in the GDGG rocks.

The baddeleyite cores in some spongy zircon grains in the HNB dykes (Fig. 8 e, f) suggest that these zircons crystallised at the expense of baddeleyite following the reaction: $ZrO_2 + SiO_2 \leftrightarrow ZrSiO_4$. The aggregate- or polycrystal-like morphology also supports this interpretation. Similar baddeleyite-zircon relationships have been identified in some metagabbros (Beckman et al., 2017) and the coexistence of baddeleyite and zircon has been observed in some coarse-grained unmetamorphosed gabbros (Heaman et al., 1992). These spongy HNB zircons analysed here show very low Th concentrations (<30 ppm, generally ~10 ppm) and Th/U (0.01–0.15), which are commonly interpreted to reflect the very low Th concentration and Th/U ratio of baddeleyite (Heaman & LeCheminant, 1993). The heterogeneous U-Pb age data of the spongy zircons may help constrain the origin of the baddeleyite. Possible options are that 1) the baddeleyites were inherited from the magma source, 2) they were assimilated from the mafic (lower) crust or 3) they crystallised during the magma ascent. Many of these spongy zircons crystallised from baddeleyite show high common Pb, however, and they were thus omitted from the age calculations. The remaining analyses show diverse ages between 2054–1844 Ma, with the largest groups around 1860 Ma, which conforms to the crystallisation ages recorded by the angular zircon population. The older ages might suggest that at least some baddeleyites were inherited from the magma source (discussed later). The baddeleyite-zircon crystallisation may have recorded magma evolution from partial melting of the magma source at low-silica conditions, where baddeleyite is the main Zr-phase, to ascent, emplacement and crystallisation of a more hydrous and silica-enriched magma. Although rare, xenocrystic baddeleyite has been shown

to survive even in upper mantle conditions (Heaman & Lecheminant, 1993; Schärer et al., 1997) indicating that such a deep inheritance is possible.

### *5.2. Petrogenesis of the rock types*

#### *5.2.1. Screening for the effect of post-magmatic alteration*

All the analysed samples show low LOI contents (0.4–2.3 wt. %; Table 1) suggesting general lack of or only weak post-magmatic alteration or metasomatism. In addition, the incompatible LILE and Ce, elements which are known to be mobile under medium-grade metamorphic conditions (e.g., Polat et al., 2002), record coherent compositions within the different groups and correlate with immobile incompatible elements such as Nb and Zr (Fig. 6). The samples show Ce/Ce* ratios between 0.9-1.1 (with one outlier showing Ce/Ce* 1.2 in the adakite-like group; Table 1) indicating limited LREE mobility (Polat et al., 2002). Petrographic studies confirm the primary nature of the samples since only minor amounts of typical secondary minerals (e.g., chlorite or epidote) were observed (Fig. 3).

#### *5.2.2. The role of fractional crystallisation*

The HMG samples show trends of pyroxene and hornblende (and possibly olivine that plots outside of Fig. 12a and b) fractionation, and accumulation in a few samples, based on the positive correlation between MgO and $Fe_2O_3^T$ and negative correlation between MgO and $Al_2O_3$ (Fig. 12). Similar trends are observed in the adakite-like rocks, but with relatively steeper MgO-$Fe_2O_3^T$ and gentler MgO-$Al_2O_3$ trends suggesting fractionation dominated by hornblende rather than pyroxene. These contrast with the HNB samples which show rather narrow ranges of $SiO_2$ and MgO contents and lack a clear correlation in MgO-$Fe_2O_3^T$ and MgO-$Al_2O_3$ spaces indicating only a minor role of fractional crystallisation in the magma evolution. Negative Eu-anomalies in some samples, however, indicate plagioclase fractionation at some point during HNB magma evolution (Fig. 7). The gabbroic HNB sample 031.1-JKA-015 shows potential evidence of magma mixing with characteristics of both HNB and HMG groups (Figs. 4, 5, 6, and 12).

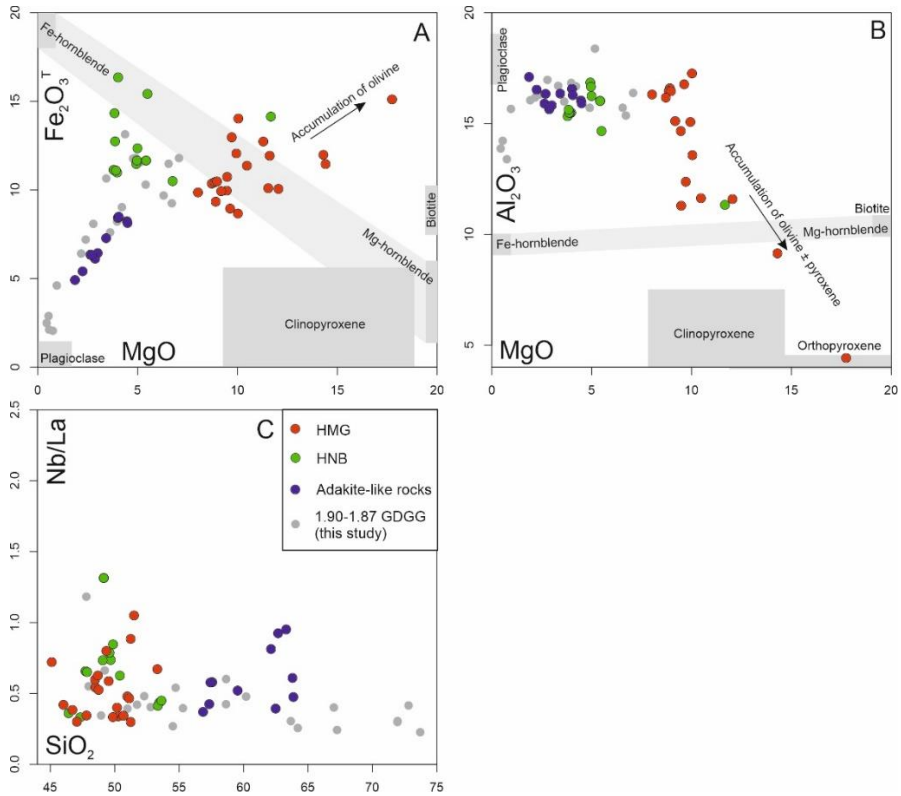


Fig. 12. Geochemical diagrams used to estimate the role of FC (A and B) and AFC (C) processes. In A and B, mineral compositions are indicated with grey boxes.

The drastically different major and trace element compositions of the HNB and HMG magmas suggest that they cannot derive from the same parental magma and must represent distinct magma sources. Origin of the adakite-like rocks after fractional crystallisation of HMG-type magma would seem possible, but lower Y and HREE concentrations and higher MREE/HREE ratios in adakite-like rocks (Fig. 7) rule out this scenario. In all, fractional crystallisation can only explain the internal compositional variation within the rock groups.

#### *5.2.3. The effect of crustal contamination*

High, mantle-like, initial $\varepsilon_{Nd}$ value and zircon $\varepsilon_{Hf}$ values argue against significant crustal contamination for HMG sample 10-MJV-02 (Figs. 10 and 11). On the other hand, inherited zircons and lower initial $\varepsilon_{Hf}$ values in magmatic zircon in sample 085.1-JKA-015 imply at least some role for such a process in this case. The negative Zr-Hf anomaly (Fig. 7), the lack of correlation between Nb/La and $SiO_2$ (Fig. 12c) and the primitive nature of the HMG imply that this role was very minor, however. The geochemical characteristics of the HMG (Fig. 13) are thus interpreted to dominantly reflect their mantle sources. Apart for being more evolved and also containing some inherited zircons, the HNB and the adakite-like samples also lack clear indications of crustal contamination during their differentiation (e.g., Fig. 12c) and we interpret that the observed trace element enrichments and depletions primarily reflect source characteristics in these cases as well (Fig. 13). It is also worth noting that the incompatible trace element contents are lower in the surrounding metasedimentary rocks (see Kähkönen, 2005) than in the studied magmatic rocks. The former are thus not very effective in altering the characteristic mantle-derived geochemical signatures of more enriched magmas by assimilation.

#### *5.2.4. Sources of the different rock groups*

We performed partial melting modelling of various mantle and crustal rocks to further constrain the sources for the different rock groups (Fig. 14). Non-modal batch melting models (Shawn, 1970) were run using several different starting compositions: 1) depleted MORB mantle peridotite (DMM; Salters and Stracke, 2004) in spinel, spinel-garnet and garnet stability fields; 2) four different types of lower crustal garnet-pyroxenite xenoliths found in the Kaavi kimberlite pipes in eastern Finland (Hölttä et al., 2000); 3) lower crustal amphibolite (Rudnick and Gao, 2003); and 4) 1.88 Ga GDGG gabbro (024-JKA-015; this study). Although not reported from the xenoliths, 1% of rutile was added to the garnet-pyroxenites in the models to study its effect on Nb-Ta fractionation. Rutile is an important phase because it is common in garnet-pyroxenites and eclogites as indicated by natural samples (Rudnick et al., 2000; Xu et al., 2006; Tang et al., 2019) and experimental data (Rapp & Watson, 1995; Pertermann & Hirschmann, 2003) and it controls nearly all Nb, Ta and a considerable amount of the Ti, Zr and Hf budgets in eclogitic, pyroxenitic and peridotitic rocks (Rudnick et al., 2000; Zack et al., 2002; Aulbach et al., 2008). Rutile has a higher partition coefficient for Nb than for Ta, which results in elevated Nb/Ta ratios in partial melts derived from sources with rutile if rutile enters the melt phase (Ryerson & Watson, 1987; Foley et al., 2000; Klemme et al., 2005). The parameters and results of the modelling can be found in Electronic Appendix F.

*GDGG*

An arc-related setting for the ~1.88 Ga GDGG is supported by several lines of evidence. The age, enrichment in subduction-mobile elements and depletion in Nb, Ta and Ti as well as several characteristic trace element ratios all argue for a subduction-related continental arc environment (Figs. 7 and 13). A similar setting has been proposed by numerous researchers for the contemporaneous magmatism in southern Finland (e.g., Nironen & Bateman, 1989; Lahtinen, 1996; Kähkönen, 2005; Kara et al., 2018). The granodiorite shows initial zircon $\varepsilon_{Hf}$ values which are similar to previously published values (Fig. 11) but the gabbro exhibit remarkably low average initial zircon

$\varepsilon_{Hf}$ of -2.8. This is the lowest average value recorded for a mafic arc rock in the SO and suggest crustal contamination or the involvement of an older crustal unit at depth (see Kara et al., 2018).

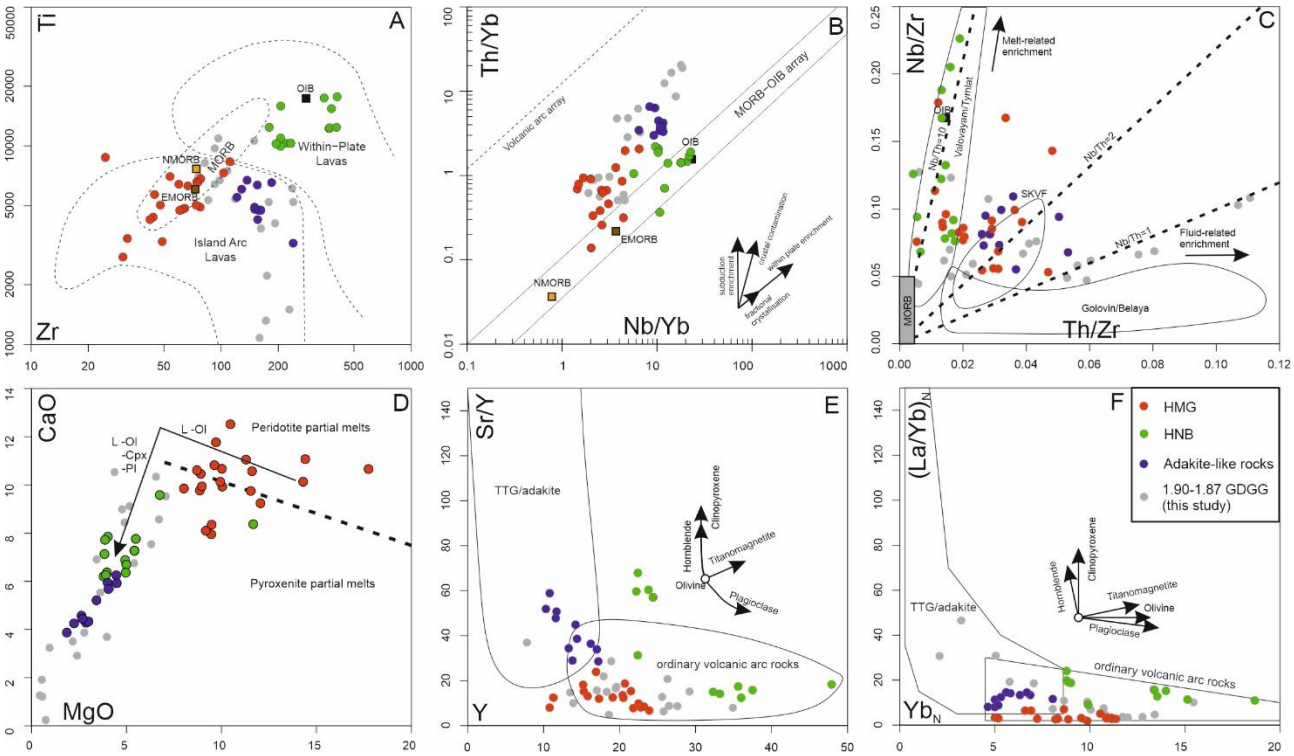


Fig. 13. Various geotectonic discrimination diagrams: A) Ti vs. Zr (Pearce, 1982); B) Th/Yb vs. Nb/Yb (Pearce, 2008); C) Nb/Zr vs Th/Zr (Kepezhinskas et al., 1997); D) CaO vs. MgO; E) Sr/Y vs. Y (Defant and Drummond, 1990); and F) (La/Yb)N/YbN (Martin, 1986). The dashed line separating peridotite- and pyroxenite-source primary magmas in D is after Herzberg (2011) and black broken arrow showing typical liquid line of descent for primary magmas that crystallise gabbro in the crust is after Herzberg and Asimow (2008).

*HMG*

A mildly depleted mantle reservoir has been proposed as a source for the synorogenic Svecofennian gabbroic magmatism and the juvenile Svecofennian 1.90−1.87 Ga crust (e.g., Lahtinen and Huhma, 1997; Rutanen et al., 2011). In general, the HMG show more depleted isotopic signatures and more primitive geochemistry compared to the synorogenic gabbros (Figs. 5, 6, 10, 11), suggesting a different source. HMG sample 10-MJV-02 shows an $\varepsilon_{Nd}$ value of +3.8 and an average zircon $\varepsilon_{Hf}$ value of +3.3 indicating that the magmas are derived from a depleted and juvenile mantle source (Figs. 10 and 11). High Cr, Ni, MgO contents and high Mg# support this hypothesis and suggest that the HMG are rather primitive melts (Figs. 5 and 6). In addition, the degree of partial melting in the source must have been rather high based on the high Cr, Ni and MgO contents. The tectonic discrimination diagrams point to a source similar to enriched mid ocean ridge basalt (E-MORB; Fig. 13a, b). On the other hand, slight enrichment in LILE, LREE, Pb and Nb-Ta depletion, pointing to a subduction component (see Pearce and Peate, 1995) suggests that the source was modified by subduction fluids (Figs. 6, 7, 13c). The considerable variation of ~10 ε-units in Hf-isotopes in sample 10-MJV-02 could indicate heterogeneous source characteristics and disequilibrium processes during crystallisation (Fig. 11). Alternatively, input from a subduction component could explain this variation by the "zircon effect", i.e., strong influence of subducted zircon-bearing sediments on the Hf-isotope signature of juvenile magmas (e.g., Patchett et al. 1984). The chondritic zircon Hf-values in sample 085.1-JKA-015 are more likely due to entrainment of zircons from the surrounding bedrock and recrystallisation of them at 1.86 Ga.

A possible origin for the HMG could be high degree partial melting of a mildly depleted mantle, i.e. a mantle (wedge) peridotite that is slightly metasomatised and enriched by subduction related fluids. Peridotitic source is also suggested by CaO-MgO systematics (Fig. 13d), since bulk partition coefficients for CaO ($D_{CaO}^{Solid/Liquid}$) are usually <1 in peridotite, which results in high CaO at a given MgO for the peridotite-derived melts (Herzberg, 2011). Our modelling shows that partial melting of DMM in the spinel-garnet stability field could represent a possible framework for the derivation of the HMG melts (Fig. 14). The suggested degree of partial melting of "pure DMM" is rather low given the high MgO, Ni, and Cr contents of HMG. Therefore, it is likely that the mantle reservoir was modified by subduction-related fluids and/or melts as shown by several trace element ratios (Figs. 13b and c). This means that higher degree partial melting is needed to achieve the HMG-like geochemical features which agrees with the high MgO, Ni and Cr content.

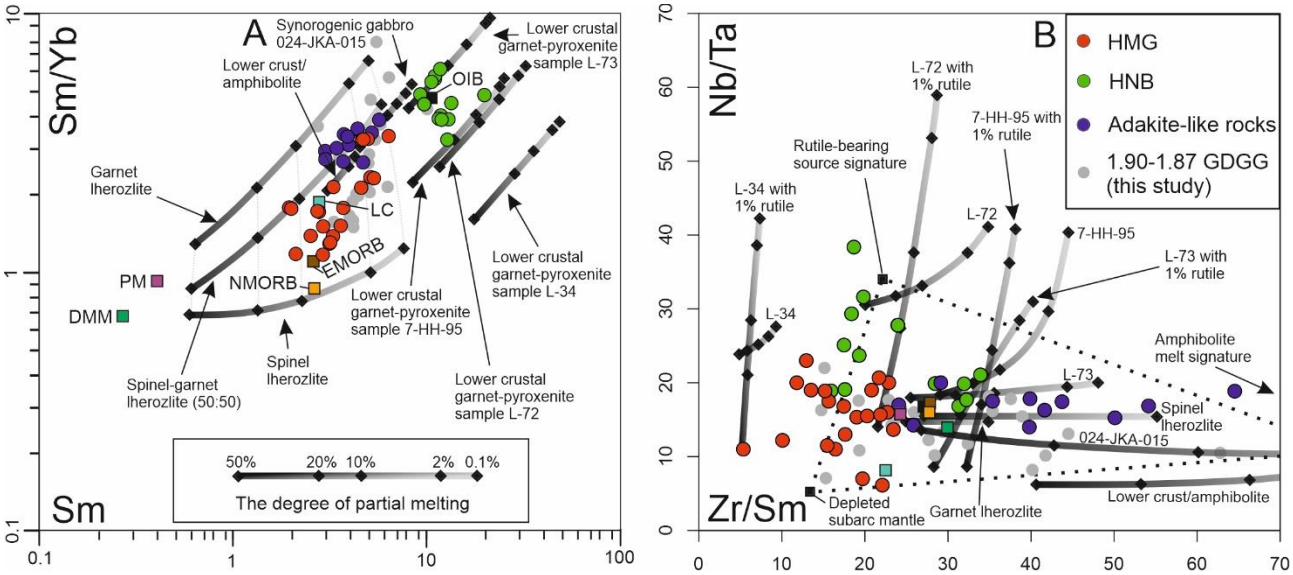


Fig. 14. Non-modal batch melting models of potential sources in A) Sm/Yb vs. Sm and B) Nb/Ta vs. Zr/Sm diagrams. DMM (Salters & Stracke, 2004), PM (McDonough, 1995), N-MORB (Sun & McDonough, 1989), E-MORB (Sun & McDonough, 1989), OIB (Sun & McDonough, 1989) and LC (lower crust; Rudnick & Gao, 2003) shown for comparison.

*HNB*

The initial $\varepsilon_{Nd}$ value of +2.4 combined with the characteristic LILE, HFSE and F enrichment of the HNB indicate a more enriched mantle source compared to that of the HMG (Figs. 10 and 13a, b). In addition, the degree of partial melting in the source may also be smaller for the HNB magmas (Figs. 6, 7, 13 and 14). Notable features in the HNB are the suprachondritic Nb/Ta and Zr/Hf (see Rudnick et al., 2000) and high Nb-content, which suggest high-pressure melting of a rutile-bearing source (see Foley et al., 2000; Klemme et al., 2005). Considering these and their other trace element characteristics, a pyroxenitic source similar to some OIBs (Hircshmann et al., 2003; Sobolev et al., 2005; Herzberg et al., 2011, 2014; Pang et al., 2019) is plausible for the HNB. In terms of major elements, the relative CaO depletion of the HNB (Fig. 13c) also points to a pyroxenitic source, since bulk distribution coefficients for CaO are usually >1 in $SiO_2$-rich residual pyroxenite (Herzberg, 2011). This results in lower CaO at a given MgO for pyroxenite derived melts compared to those of peridotite-derived melts (cf. HMG). The lower Fe/Mn ratio (Table 1) in the HMG (58.1 on average) compared to the HNB (67.6 on average), further indicate that the two groups had different sources in terms of modal composition (see Sobolev et al., 2005).

The modelling shows that melting of lower crustal garnet-bearing pyroxenite with composition similar to the Kaavi xenoliths could produce magmas with HNB trace element characteristics (Fig. 14). Without rutile in the source, the Nb/Ta observed in the HNB samples are only achieved with

relatively high degrees of partial melting (e.g., >40% implied for L-72 source), however. Addition of 1% rutile to the models lowers the implied degrees of partial melting and the partial melting trends show much better fits with the HNB data in general. Therefore, the source is expected to contain rutile, which is transferred to the melt phase. The high HFSE concentrations in the HNB also support this scenario (see Rudnick et al., 2000; Zack et al., 2002; Aulbach et al., 2008).

The zircon Hf-isotopes record some variation with average $\varepsilon_{Hf}$ values of -1.6 and -2.3 and a total range of 13 and 9.4 ε-units for 033.1- and 033.3-JKA-015, respectively. The contrast in Nd and Hf isotopes and the large variation in $\varepsilon_{Hf}$ values can be explained by several different ways: 1) crustal assimilation and magma mixing (e.g., Belousova et al., 2006), 2) source heterogeneities (e.g., Andersson et al., 2011; Couzinié et al., 2016), 3) disequilibrium partial melting of the source (e.g., Tang et al., 2014), or 4) "zircon effect" (Patchett et al., 1984) i.e. inheritance of zircon, baddeleyite (e.g., Schärer et al., 1997; this study) or rutile (see Aulbach et al., 2008), which are the main carriers of Hf. It may also be a combination of these processes, which we suggest here for the HNB. Firstly, the lower crustal garnet-pyroxenite source rocks, i.e., arclogites, have formed during a rather long timespan (Peltonen et al., 2006), and secondly, via subduction they contain material, especially zircons, eroded from the surrounding older Svecofennian or possibly even Archean rocks (e.g., Huhma et al., 1991; Lahtinen et al., 2009b). These zircons carrying unradiogenic Hf are transformed into baddeleyites during arclogite formation (discussed below), which is suggested by baddeleyite cores found in spongy zircons and negative $\varepsilon_{Hf}$ values in all but one recrystallised spongy zircon. Thirdly, disequilibrium melting of such a heterogeneous source would lead to variable Hf isotope compositions, such as those observed in the HNB zircons.

*Adakite-like rocks*

The high Sr and LREE and low Y and HREE concentrations in the adakite-like samples indicate a source with residual garnet whereas plagioclase (if present) entered the melt phase. In addition, the samples show elevated $Al_2O_3$ and $Na_2O$ content a petrogenesis similar to adakites or adakite-like rocks elsewhere. In general, three mechanisms have been proposed to generate an adakitic geochemical signature: 1) partial melting of young and hot subducting basaltic slab material under eclogite-facies conditions where garnet remains in the residuum (adakites ss. or high-silica adakites; Defand & Drummond, 1990; Martin et al., 2005), 2) partial melting of mafic lower crust under eclogite-facies conditions (e.g., Atherton and Petford, 1993; Moyen, 2009) or 3) assimilation and fractional crystallisation (AFC) of "normal" mafic arc magmas (e.g., Macpherson et al., 2006). Absence of 1.86 Ga "normal" arc type rocks and distinctive REE-characteristics between the HMG and adakite-like rocks argue against the AFC origin. The "adakite-signature" is not particularly strong in these samples, which is best explained by high pressure melting of a lower crustal source. Melt modelling in this study argues for a mafic lower crustal or garnet-amphibolite source (Fig. 14), similar to the model suggested by Väisänen et al. (2012) for a 1.87 Ga TTG rock assemblage found 100 km SW of the present study area.

The adakite-like sample 026.1-JKA-015 exhibits a high initial $\varepsilon_{Nd}$ value of +3.1 suggesting a rather juvenile source. In contrast, the average zircon $\varepsilon_{Hf}$ value is -4.0 with single analyses varying between -8.1 and +0.3 and showing one outlier of -12.6. An important observation is that the 1.88 Ga GDGG gabbro sample (024.1-JKA-015) shows identical zircon $\varepsilon_{Hf}$ values and Th/U ratios with the adakite-like sample. This, and the two inherited 1888 Ma and 1885 Ma grains in the adakite-like sample suggest that the lower crustal source could have a composition and age similar to the synorogenic gabbros. This interpretation is supported by modelling of partial melting since a very good fit is achieved using the composition of the GDGG gabbro sample as the source (Fig. 14). Moreover, uniform zircon Th/U ratios in inherited and magmatic grains indicate that all the zircons might have been inherited from this same source. The zircons were then subsequently recrystallised during

magma emplacement. The subduction-related enrichment is evident in the adakite-like samples based on their trace element characteristics, especially in terms of trace element ratios such as Th/Yb and Zr/Y (Figs. 7 and 13). This is plausible since the synorogenic magmas were formed in a volcanic arc setting 20 Ma earlier.

*5.3. Formation, delamination and partial melting of arclogites during the Svecofennian orogeny*

The tectono-magmatic model proposed here is based on the recent hypotheses of the formation and delamination cycle of arclogites beneath continental arcs as a result of intracrustal differentiation of calc-alkaline silicic arc magmas that leave behind mafic garnet-pyroxenite cumulates (Lee et al., 2006; Lee & Anderson, 2015; Tang et al., 2018). We suggest the following sequence as a model for the Svecofennian orogeny at 1.90–1.86 Ga (Fig. 15a and b): 1) formation of rutile-bearing arclogites as a result of the voluminous and abundant 1.90–1.87 Ga calc-alkaline GDGG magmatism; 2) partial delamination of the rutile-bearing arclogites triggered by an extensional tectonic regime (Lahtinen, 2005), the high density of the arclogites (Lee et al., 2006) and hot and viscous upper mantle (Kukkonen et al., 2008); 3) upwelling of juvenile and subduction-modified mantle (wedge) peridotite; and 4) partial melting of the rutile-bearing arclogites to generate the HNB magmas, partial melting of the mantle (wedge) peridotite to generate the HMG magmas and partial melting of the mafic lower crust to generate the adakite-like rocks (Fig. 15b). The timespan of the growth and delamination of the arclogite layer, approximately 20–30 Myr, agrees with the model of Lee et al. (2006). We suggest that the delamination triggered the entire partial melting sequence of the different source lithologies. Upwelling of hot upper mantle peridotite into the "void" after delaminated arclogite brought heat to the lower crust, which caused partial melting of the arclogites and of the lower crust.

The suggested model explains several features of the 1.86 Ga rock association in the SO. Firstly, rutile- and garnet-bearing pyroxenites are the likely source for the elevated Nb, Nb/Ta and OIB-like geochemical features in the HNB. The previously described ~1.86 Ga mafic intrusions from southern Finland (Väisänen et al., 2012a, 2012b; Nevalainen et al., 2014) seem to share the same features. Moreover, the high Nb/Ta in the ~1.86 Ga HNB magmas seem to balance the low Nb/Ta observed in ~1.88 Ga arc rocks elsewhere in southern Finland (Fig. 15c and d), suggesting that arclogites are important as a Nb-reservoir and in fractionating Nb/Ta during continental arc magmatism (Tang et al., 2019). Secondly, it explains the genetic link between the HNB, HMG and adakite-like rocks. Nevalainen et al. (2014) observed more primitive gabbros associated with enriched monzogabbros, whereas Väisänen et al. (2012b) described TTG- and adakite-like magmas associated with enriched diorites. These enriched monzogabbros and diorites are similar to HNB, which is a strong indication that identical processes were ongoing simultaneously in southern Finland. Moreover, a statistical study by Ruotoistenmäki (2019) showed that magmatic rocks with an adakitic signature might be more abundant among the Svecofennian rocks than previously suggested. This implies that the arclogite model can be extended to cover the whole south-central Fennoscandian shield. Thirdly, it explains the extremely thick crust and HVLC encountered in Central and Southern Svecofennia (Luosto et al., 1991; Korja et al., 1993) by (partial) stabilization of the dense arclogite layer (Fig. 1 and 14). A similar hypothesis, although explained by delamination of eclogitic lower crust, was presented by Kukkonen et al. (2008) to account for the HVLC in the central part of the Fennoscandian shield within the Archean-Proterozoic boundary zone in eastern Finland. Finally, our model suggests that the crustal thickening started already at 1.90 Ga by arclogite formation and Andean type magmatic vertical accretion (see Cawood et al., 2009). The arclogite hypothesis supports the model described by Hermansson et al. (2008) with subduction beneath a single active continental margin in combination with hinge retreat and advance at 1.90–1.86 Ga.

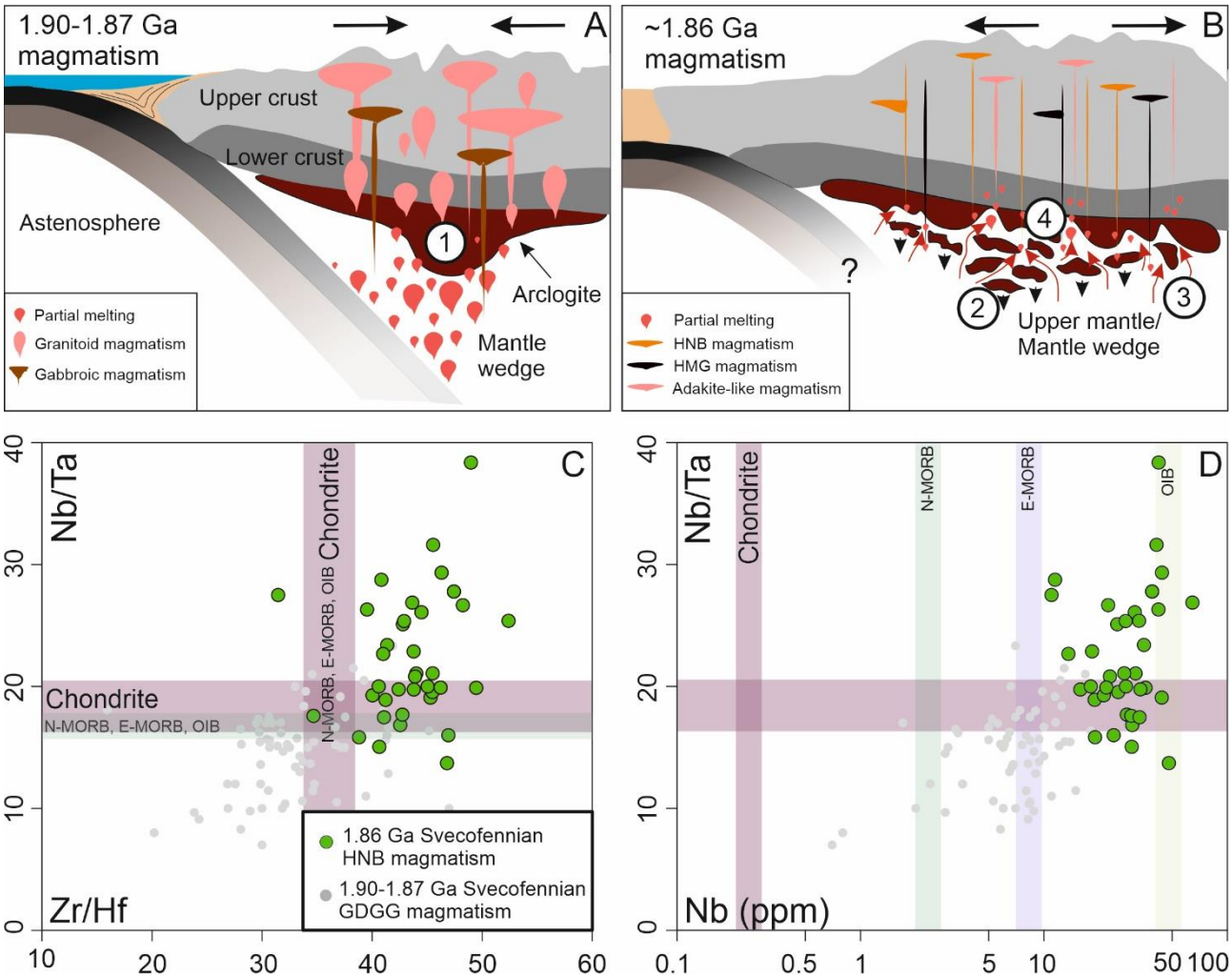


Fig. 15. A) and B) Schematic diagram of the arclogite model for the Svecofennian orogen at 1.90-1.86 Ga. 1) Growth of the arclogite layer complementary to the voluminous calc-alkaline felsic magmatism, 2) (partial) delamination of the dense arclogite layer and partial melting of the arclogites to produce the HNB magmas, 3) upwelling and partial melting of the upper mantle to produce the HMG magmas, 4) partial melting of the lower crust to produce the adakite-like magmas. C) Zr/Hf vs. Nb/Ta and D) Nb vs. Nb/Ta data for 1.86 Ga HNB magmatism and 1.90-1.87 Ga GDGG magmatism from Southern Svecofennia. HNB data from this study, Väisänen et al. (2012a, 2012b) and Nevalainen et al. (2014); GDGG data from this study and Kara et al. (2018).

### *5.4. Implications to Precambrian orogens*

Mature continental arcs, where the upper plate is continental lithosphere and/or accreted transitional lithosphere, usually exhibit crustal thicknesses of >50 km (Andersson, 2005; Ducea et al., 2015). This can be considered as a loose threshold value for deep intracrustal magma differentiation (see Farner & Lee, 2017). Globally, areas with crustal thicknesses of >50 km cover about 10% of the shield areas (Mooney et al., 1998) and geophysical studies reveal HVLC in several areas, such as the Precambrian basement of the East European Craton (e.g., Bogdanova et al., 2006), western North America (Cloves et al., 2002) and North Australia (Goncharov et al., 1998). Our study together with direct evidence of lower crustal garnet-pyroxenite xenoliths (Hölttä et al., 2000; Peltonen et al., 2006) suggests that the formation, delamination and partial melting of arclogites in Precambrian orogens might be a "normal" phenomenon rather than a special case, especially within thick continental arcs. The problem in the study of arclogites is the rarity of direct evidence of such rocks (Lee et al., 2006). However, their possible melting products, i.e., the HNB from this study, combined with geophysical data are plausible ways to trace their existence.

## 6. Conclusion

A 1.86 Ga rock association including rare high-Nb gabbros, high-Mg gabbros and adakite-like rocks occurs in the central part of the Fennoscandian shield. Its ages and geochemical characteristics are clearly different from the adjacent, 1.90–1.87 Ga, calc-alkaline igneous rocks with volcanic arc affinities.

We suggest the following geodynamic model for the change in the magmatic environment and for the genesis of the 1.86 Ga magmas: 1) formation of rutile-bearing lower crustal garnet-pyroxenite layer, i.e., arclogite, as a result of the voluminous and abundant 1.90–1.87 Ga calc-alkaline felsic magmatism; 2) partial delamination of the rutile-bearing arclogites triggered by an extensional tectonic regime, the high density of the arclogites, and the presence of hot and viscous upper mantle; 3) upwelling of the juvenile and subduction-modified mantle (wedge) peridotite; and 4) partial melting of the rutile-bearing arclogites to generate the high-Nb magmas, partial melting of the mantle (wedge) peridotite to generate the high-Mg magmas and partial melting of the mafic lower crust to generate the adakite-like rocks. This model explains the extremely thick crust and high velocity lower crust encountered in central Fennoscandian Shield by partial stabilization of the dense arclogite layer.

This study presents a new possible mechanism for the generation of high-Nb basalts/gabbros by partial melting of rutile-bearing arclogites beneath thickened arc crust and is the first possible example of arclogite formation in a Paleoproterozoic orogen.

**Acknowledgements**

J. Kara was funded by grant from the Turku University Foundation and the field work was funded by a grant from the Finnish Society of Sciences and Letters. Funding for J.S. Heinonen was provided by the Academy of Finland (Grant no. 295129). Arto Peltola is thanked for making the zircon and monazite epoxy mounts. This is a Finnish Geosciences Research Laboratory contribution. We appreciated the thorough reviews of Åke Johansson and James Worthington, and suggestion by the Editor Xian-Hua Li, which helped to improve the manuscript.

**Supplementary Electronic material**

A: Methods
B: Whole rock geochemical data
C: Zircon and monazite U-Pb data
D: U-Pb data interpretation
E: Zircon Lu-H data
F: Melt modelling

**References**

Anderson, D. L., 2005. Large Igneous Provinces, Delamination, and Fertile Mantle. Elements, 1, 271–275. https://doi.org/10.2113/gselements.1.5.271

Andersson, U. B., Begg, G. C., Griffin, W. L., & Högdahl, K., 2011. Ancient and juvenile components in the continental crust and mantle: Hf isotopes in zircon from Svecofennian magmatic rocks and rapakivi granites in Sweden. Lithosphere, 3, 409-419. https://doi.org/10.1130/L162.1

Atherton, M. P., & Petford, N., 1993. Generation of sodium-rich magmas from newly underplated basaltic crust. Nature, 362, 144-146. https://doi.org/10.1038/362144a0

Aulbach, S., O'Reilly, S. Y., Griffin, W. L., & Pearson, N. J., 2008. Subcontinental lithospheric mantle origin of high niobium/tantalum ratios in eclogites. Nature Geoscience, 1, 468–472. https://doi.org/10.1038/ngeo226

Bas, M. J. L., Maitre, R. W. L., Streckeisen, A., & Zanettin, B., 1986. A chemical classification of volcanic rocks based on the total alkali-silica diagram. Journal of Petrology, 27, 745–750.

https://doi.org/10.1093/petrology/27.3.745

Beckman, V., Möller, C., Söderlund, U., & Andersson, J., 2017. Zircon growth during progressive recrystallization of Gabbro to Garnet Amphibolite, Eastern Segment, Sveconorwegian orogen. Journal of Petrology, 58, 167–188. https://doi.org/10.1093/petrology/egx009

Bedrock of Finland - DigiKP. Digital map database [Electronic resource]. Espoo: Geological Survey of Finland [referred 19.09.2019]. Version 2.0.

Belousova, E. A., Griffin, W. L., & O'Reilly, S. Y., 2006. Zircon crystal morphology, trace element signatures and Hf isotope composition as a tool for petrogenetic modelling: examples from Eastern Australian granitoids. Journal of Petrology, 47, 329-353. https://doi.org/10.1093/petrology/egi077

Bergman, S., Högdahl, K., Nironen, M., Ogenhall, E., Sjöström, H., Lundqvist, L., & Lahtinen, R., 2008. Timing of Palaeoproterozoic intra-orogenic sedimentation in the central Fennoscandian Shield; evidence from detrital zircon in metasandstone. Precambrian Research, 161, 231–249. https://doi.org/10.1016/j.precamres.2007.08.007

Bogdanova, S., Gorbatschev, R., Grad, M., Janik, T., Guterch, A., Kozlovskaya, E., Motuza, G., Skridlaite, G., Starostenko, V., Taran, L., EUROBRIDGE, POLONAISE WORKING GROUPS, 2006. EUROBRIDGE: new insight into the geodynamic evolution of the the East European Craton. In: Gee, D.G., Stephenson, R.A. (Eds.), European Lithosphere Dynamics. Memoirs, 32. Geological Society, London, 599–625. https://doi.org/10.1144/GSL.MEM.2006.032.01.36

Boynton, W. V., 1984. Cosmochemistry of the rare earth elements: meteorite studies. In: Developments in geochemistry, 2, 63-114. Elsevier. https://doi.org/10.1016/B978-0-444-42148-7.50008-3

Castillo, P. R. 2008. Origin of the adakite-high-Nb basalt association and its implications for postsubduction magmatism in Baja California, Mexico. Bulletin of the Geological Society of America, 120 (3–4), 451–462. https://doi.org/10.1130/B26166.1

Castillo, P. R. 2012. Adakite petrogenesis. Lithos, 134–135, 304–316. https://doi.org/10.1016/j.lithos.2011.09.013

Cawood, P. A., Kröner, A., Collins, W. J., Kusky, T. M., Mooney, W. D., & Windley, B. F., 2009. Accretionary orogens through Earth history. Geological Society, London, Special Publications, 318, 1-36. ttps://doi.org/10.1144/SP318.1

Clowes, R. M., Burianyk, M. J., Gorman, A. R., & Kanasewich, E. R., 2002. Crustal velocity structure from SAREX, the southern Alberta refraction experiment. Canadian Journal of Earth Sciences, 39, 351-373. https://doi.org/10.1139/e01-070

Couzinié, S., Laurent, O., Moyen, J. F., Zeh, A., Bouilhol, P., & Villaros, A., 2016. Post-collisional magmatism: crustal growth not identified by zircon Hf–O isotopes. Earth and Planetary Science Letters, 456, 182-195. https://doi.org/10.1016/j.epsl.2016.09.033

Dahlin, P., Johansson, A., & Andersson, U. B., 2014. Source character, mixing, fractionation and alkali metasomatism in Palaeoproterozoic greenstone dykes, Dannemora area, NE Bergslagen region, Sweden. Geological Magazine, 151, 573–590. https://doi.org/10.1017/S0016756813000551

Defand, M. J., & Drummond, M. S., 1990. Derivation of some modern arc magmas by melting of young subducted lithosphere. Nature, 347, 662–665. https://doi.org/10.1016/0021-9797(80)90501-9

Defant, M. J., Jackson, T. E., Drummond, M. S., De Boer, J. Z., Bellon, H., Feigenson, M. D., ... & Stewart, R. H. 1992. The geochemistry of young volcanism throughout western Panama and southeastern Costa Rica: an overview. Journal of the Geological Society, 149, 569-579. https://doi.org/10.1144/gsjgs.149.4.0569

Drummond, B. J., & Collins, C. D. N., 1986. Seismic evidence for underplating of the lower continental crust of Australia. Earth and Planetary Science Letters, 79, 361-372.

https://doi.org/10.1016/0012-821X(86)90192-5

Ducea, M. N., & Saleeby, J. B. 1996. Buoyancy sources for a large, unrooted mountain range, the Sierra Nevada, California: Evidence from xenolith thermobarometry. Journal of Geophysical Research: Solid Earth, 101, 8229–8244. https://doi.org/10.1029/95JB03452

Ducea, M. N., Saleeby, J. B., & Bergantz, G., 2015. The architecture, chemistry, and evolution of continental magmatic arcs. Annual Review of Earth and Planetary Sciences, 43, 299-331. https://doi.org/10.1146/annurev-earth-060614-105049

Farner, M. J., & Lee, C. T. A., 2017. Effects of crustal thickness on magmatic differentiation in subduction zone volcanism: a global study. Earth and Planetary Science Letters, 470, 96-107. https://doi.org/10.1016/j.epsl.2017.04.025

Foley, S. F., Barth, M. G., & Jenner, G. A., 2000. Rutile/melt partition coefficients for trace elements and an assessment of the influence of rutile on the trace element characteristics of subduction zone magmas. Geochimica et Cosmochimica Acta, 64, 933–938. https://doi.org/10.1016/S0016-7037(99)00355-5

Gorbatschev, R., & Bogdanova, S., 1993. Frontiers in the Baltic Shield. Precambrian Research, 64, 3–21. https://doi.org/10.1016/0301-9268(93)90066-B

Hakkarainen, G., 1994. Geology and geochemistry of the Hämeenlinna-Somero volcanic belt, southwestern Finland: a Paleoproterozoic island arc. In: Geochemistry of Proterozoic supracrustal rocks in Finland. Geological Survey of Finland, Special Paper, 19, 85–100.

Halkoaho, T., Ahven, M., Rämö, O. T., Hokka, J., & Huhma, H., 2020. Petrography, geochemistry, and geochronology of the Sc-enriched Kiviniemi ferrodiorite intrusion, eastern Finland. Mineralium Deposita, 1-20. https://doi.org/10.1007/s00126-020-00952-2

Hastie, A. R., Mitchell, S. F., Kerr, A. C., Minifie, M. J., & Millar, I. L. 2011. Geochemistry of rare high-Nb basalt lavas: Are they derived from a mantle wedge metasomatised by slab melts?. Geochimica et Cosmochimica Acta, 75, 5049-5072. https://doi.org/10.1016/j.gca.2011.06.018

Hawkesworth, C. J., Gallagher, K., Hergt, J. M., & McDermott, F., 1993. Mantle and slab contributions in arc magmas. Annual Review of Earth and Planetary Sciences, 21, 175-204. https://doi.org/10.1146/annurev.ea.21.050193.001135

Heaman, L., LeCheminant, A., & Rainbird, R., 1992. Nature and timing of Franklin igneous events, Canada: implications for a Late Proterozoic mantle plume and the break-up of Laurentia. Earth and Planetary Science Letters, 109, 117–131. https://doi.org/10.1016/0012-821X(92)90078-A

Heaman, L. M., & LeCheminant, A. N., 1993. Paragenesis and U-Pb systematics of baddeleyite (ZrO2). Chemical Geology, 110, 95–126. https://doi.org/10.1016/0009-2541(93)90249-I

Hermansson, T., Stephens, M. B., Corfu, F., Page, L. M., & Andersson, J., 2008. Migratory tectonic switching, western Svecofennian orogen, central Sweden: Constraints from U/Pb zircon and titanite geochronology. Precambrian Research, 161, 250–278. https://doi.org/10.1016/j.precamres.2007.08.008

Herzberg, C., 2011. Identification of Source Lithology in the Hawaiian and Canary Islands: Implications for Origins. Journal of Petrology, 52, 113–146, https://doi.org/10.1093/petrology/egq075

Herzberg, C., Cabral, R. A., Jackson, M. G., Vidito, C., Day, J. M. D., & Hauri, E. H., 2014. Phantom Archean crust in Mangaia hotspot lavas and the meaning of heterogeneous mantle. Earth and Planetary Science Letters, 396, 97-106. https://doi.org/10.1016/j.epsl.2014.03.065

Hirschmann, M. M., Kogiso, T., Baker, M. B., & Stolper, E. M., 2003. Alkalic magmas generated by partial melting of garnet pyroxenite. Geology, 31, 481–484. https://doi.org/10.1130/0091-7613(2003)031<0481:AMGBPM>2.0.CO;2

Hölttä, P., Huhma, H., Mänttäri, I., Peltonen, P., & Juhanoja, J., 2000. Petrology and geochemistry of mafic granulite xenoliths from the Lahtojoki kimberlite pipe, eastern Finland. Lithos, 51, 109-133. https://doi.org/10.1016/S0024-4937(99)00077-8

Huhma, H., Claesson, S., Kinny, P. D., & Williams, I. S., 1991. The growth of Early Proterozoic

crust: new evidence from Svecofennian detrital zircons. Terra Nova, 3, 175-178. https://doi.org/10.1111/j.1365-3121.1991.tb00870.x

Janoušek, V., Farrow, C. M., & Erban, V., 2006. Interpretation of whole-rock geochemical data in igneous geochemistry: Introducing Geochemical Data Toolkit (GCDkit). Journal of Petrology, 47, 1255–1259. https://doi.org/10.1093/petrology/egl013

Johansson, Å., & Karlsson, A., 2020. The "intraorogenic" Svecofennian Herräng mafic dyke swarm in east-central Sweden: age, geochemistry and tectonic significance. GFF, 142, 1-22. https://doi.org/10.1080/11035897.2019.1708450

Kähkönen, Y., Huhma, H., & Aro, K., 1989. U-Pb zircon ages and Rb-Sr whole-rock isotope studies of early Proterozoic volcanic and plutonic rocks near Tampere, southern Finland. Precambrian Research, 45, 27-43. https://doi.org/10.1016/0301-9268(89)90029-6

Kähkönen, Y., 2005. Svecofennian Supracrustal Rocks. Developments in Precambrian Geology, 14, 343–405. https://doi.org/https://doi.org/10.1016/S0166-2635(05)80009-X

Kara, J., Väisänen, M., Johansson, Lahaye, Y., O'Brien, H., & Eklund, O., 2018. 1.90-1.88Ga arc magmatism of central Fennoscandia: Geochemistry, U-Pb geochronology, Sm-Nd and Lu-Hf isotope systematics of plutonic-volcanic rocks from southern Finland. Geologica Acta, 16, 1–23. https://doi.org/10.1344/GeologicaActa2018.16.1.1

Kärkkäinen, N., 1999. The age of the Koivusaarenneva ilmenite gabbro, western Finland. Geological Survey of Finland, Special Paper 27, 35-38.

Kay, R. W., & Kay, S. M., 1988. Crustal recycling and the Aleutian arc. Geochimica et Cosmochimica Acta, 52, 1351-1359. https://doi.org/10.1016/0016-7037(88)90206-2

Kay, R. W., & Kay, S. M., 1993. Delamination and delamination magmatism. Tectonophysics, 219, 177-189. https://doi.org/10.1016/0040-1951(93)90295-U

Kepezhinskas, P. K., Defant, M. J., & Drummond, M. S., 1995. Na metasomatism in the island-arc mantle by slab melt—peridotite interaction: evidence from mantle xenoliths in the North Kamchatka Arc. Journal of Petrology, 36, 1505-1527. https://doi.org/10.1093/oxfordjournals.petrology.a037263

Kepezhinskas, P., McDermott, F., Defant, M. J., Hochstaedter, A., Drummond, M. S., Hawkesworth, C. J., ... & Bellon, H., 1997. Trace element and Sr-Nd-Pb isotopic constraints on a three-component model of Kamchatka Arc petrogenesis. Geochimica et Cosmochimica Acta, 61, 577-600. https://doi.org/10.1016/S0016-7037(96)00349-3

Kilpeläinen, T., 1998. Evolution and 3D modeling of structural and metamorphic patterns of the Paleoproterozoic crust in the Tampere-Vammala area, southern Finland. Geological Survey of Finland, Bulletin, 397, 1-124.

Klemme, S., Prowatke, S., Hametner, K., & Günther, D., 2005. Partitioning of trace elements between rutile and silicate melts: Implications for subduction zones. Geochimica et Cosmochimica Acta, 69, 2361–2371. https://doi.org/10.1016/J.GCA.2004.11.015

Kogiso, T., Hirschmann, M. M., & Frost, D. J., 2003. High-pressure partial melting of garnet pyroxenite: Possible mafic lithologies in the source of ocean island basalts. Earth and Planetary Science Letters, 216, 603–617. https://doi.org/10.1016/S0012-821X(03)00538-7

Koistinen, T. J., 1981. Structural evolution of an early Proterozoic strata-bound Cu-Co-Zn deposit, Outokumpu, Finland. Transactions of the Royal Society of Edinburgh: Earth Sciences, 72, 115–158. https://doi.org/10.1017/S0263593300009949

Koistinen, T., Stephens, M.B., Bogatchev, V., Nordgulen, Ø.,Wennerström, M., Korhonen, J., 2001. Geological map of the Fennoscandian Shield, scale 1:2000 000. Geological Surveys of Finland, Norway and Sweden and the North-West Department of Natural Resources of Russia.

Korja, A., Korja, T., Luosto, U., & Heikkinen, P., 1993. Seismic and geoelectric evidence for collisional and extensional events in the Fennoscandian Shield implications for Precambrian crustal evolution. Tectonophysics, 219, 129–152. https://doi.org/10.1016/0040-1951(93)90292-R

Korsman, K., Koistinen, T., Kohonen, J., Wennerström, M., Ekdahl, E., Honkamo, M., Idman, H., & Pekkala, Y., 1997. Bedrock map of Finland 1:1 000 000. Espoo, Finland.

Kukkonen, I.T., Heikkinen, P., Ekdahl, E., Hjelt, S.-E., Yliniemi, J., Jalkanen, E., FIRE Working Group, 2006. Acquisition and geophysical characteristics of reflection seismic data on FIRE transects, Fennoscandian Shield. In: Kukkonen, I.T., Lahtinen, R. (Eds.), Finnish Reflection Experiment 2001–2005. Geological Survey of Finland, Special Paper, 43, 13–43.

Kukkonen, I. T., Kuusisto, M., Lehtonen, M., & Peltonen, P., 2008. Delamination of eclogitized lower crust: control on the crust–mantle boundary in the central Fennoscandian shield. Tectonophysics, 457, 111-127. https://doi.org/10.1016/j.tecto.2008.04.029

Lahtinen, R., 1994. Crustal evolution of the Svecofennian and Karelian domains during 2.1-1.79 Ga, with special emphasis on the geochemistry and origin of 1.93-1.91 Ga gneissic tonalites and associated supracrustal rocks in the Rautalampi area, central Finland. Geological Survey of Finland, Bulletin, 378, 1–128.

Lahtinen, R., 1996. Geochemistry of Palaeoproterozoic supracrustal and plutonic rocks in the Tampere-Hämeenlinna area, southern Finland. Geological Survey of Finland, Bulletin, 389, 1–113.

Lahtinen, R., & Huhma, H., 1997. Isotopic and geochemical constraints on the evolution of the 1.93-1.79 Ga Svecofennian crust and mantle in Finland. Precambrian Research, 82, 13–34. https://doi.org/10.1016/S0301-9268(96)00062-9

Lahtinen, R., Korja, A., & Nironen, M., 2005. Paleoproterozoic tectonic evolution. Precambrian Geology of Finland, 481–532. https://doi.org/http://dx.doi.org/10.1016/S0166-2635(05)80012-X

Lahtinen, R., Korja, A., Nironen, M., & Heikkinen, P., 2009a. Palaeoproterozoic accretionary processes in Fennoscandia. Geological Society, London, Special Publications, 318, 237–256. https://doi.org/10.1144/SP318.8

Lahtinen, R., Huhma, H., Kähkönen, Y., & Mänttäri, I., 2009b. Paleoproterozoic sediment recycling during multiphase orogenic evolution in Fennoscandia, the Tampere and Pirkanmaa belts, Finland. Precambrian Research, 174, 310–336. https://doi.org/10.1016/j.precamres.2009.08.008

Lee, C. T. A., Cheng, X., & Horodyskyj, U., 2006. The development and refinement of continental arcs by primary basaltic magmatism, garnet pyroxenite accumulation, basaltic recharge and delamination: insights from the Sierra Nevada, California. Contributions to Mineralogy and Petrology, 151, 222–242. https://doi.org/10.1007/s00410-005-0056-1

Lee, C. T. A., Morton, D. M., Kistler, R. W., & Baird, A. K., 2007. Petrology and tectonics of Phanerozoic continent formation: From island arcs to accretion and continental arc magmatism. Earth and Planetary Science Letters, 263, 370-387. https://doi.org/10.1016/j.epsl.2007.09.025

Lee, C. T. A., & Anderson, D. L., 2015. Continental crust formation at arcs, the arclogite "delamination" cycle, and one origin for fertile melting anomalies in the mantle. Science Bulletin, 60, 1141–1156. https://doi.org/10.1007/s11434-015-0828-6

Luosto, U., 1991. Moho depthmap of the Fennoscandian Shield based on seismic refraction data. In: Korhonen, H., Lipponen, A. (Eds.), Structure and Dynamics of the Fennoscandian Lithosphere. Proceedings of the Second Workshop on Investigation of the Lithosphere in the Fennoscandian Shield by Seismological Methods. Intitute of Seismology, University of Helsinki, Report, S-25, 43–49.

Macpherson, C. G., Dreher, S. T., & Thirlwall, M. F., 2006. Adakites without slab melting: high pressure differentiation of island arc magma, Mindanao, the Philippines. Earth and Planetary Science Letters, 243, 581-593. https://doi.org/10.1016/j.epsl.2005.12.034

Martin, H., 1986. Effect of steeper Archean geothermal gradient on geochemistry of subduction-zone magmas. Geology, 14, 753-756. https://doi.org/10.1130/0091-7613(1986)14<753:EOSAGG>2.0.CO;2

Martin, H., Smithies, R. H., Rapp, R., Moyen, J. F., & Champion, D., 2005. An overview of adakite,

tonalite-trondhjemiten-granodiorite (TTG), and sanukitoid: Relationships and some implications for crustal evolution. Lithos, 79, 1–24. https://doi.org/10.1016/j.lithos.2004.04.048

McKenzie, D., & O'Nions, R. K. 1983. Mantle reservoirs and ocean island basalts. Nature, 301, 229–231. https://doi.org/10.1038/301229a0

Middlemost, E. A. K., 1994. Naming materials in the magma/igneous rock system. Earth Science Reviews, 37, 215–224. https://doi.org/10.1016/0012-8252(94)90029-9

Mooney, W. D., Laske, G., & Masters, T. G., 1998. CRUST 5.1: A global crustal model at 5× 5. Journal of Geophysical Research: Solid Earth, 103, 727-747. https://doi.org/10.1029/97JB02122

Moyen, J. F., 2009. High Sr/Y and La/Yb ratios: The meaning of the "adakitic signature." Lithos, 112, 556–574. https://doi.org/10.1016/j.lithos.2009.04.001

Mäkitie, H., Kärkkäinen, N., Sipilä, P., Tiainen, M., Kujala, H., & Klami, J., 2016. Hämeen vyöhykkeen granitoidien luokittelu. Geological Survey of Finland, Archieve Report, 33, 1-146.

Nevalainen, J., Väisänen, M., Lahaye, Y., Heilimo, E., & Fröjdö, S., 2014. Svecofennian intra-orogenic gabbroic magmatism: A case study from Turku, southwestern Finland. Bulletin of the Geological Society of Finland, 86, 93–112.

Nironen, M., & Bateman, R., 1989. Petrogenesis and syntectonic emplacement in the early Proterozoic of south-central Finland: a reversely zoned diorite-granodiorite and a granite. Geologische Rundschau, 78, 617–631. https://doi.org/10.1007/BF01776194

Nironen, M., Elliott, B. A., & Rämö, O. T., 2000. 1.88-1.87 Ga post-kinematic intrusions of the Central Finland Granitoid Complex: A shift from C-type to A-type magmatism during lithospheric convergence. Lithos, 53, 37–58. https://doi.org/10.1016/S0024-4937(00)00007-4

Nironen, M., 2005. Proterozoic orogenic granitoid rocks. Developments in Precambrian Geology, 14, 443–479. https://doi.org/https://doi.org/10.1016/S0166-2635(05)80011-8

Pang, C. J., Wang, X. C., Li, C. F., Wilde, S. A., & Tian, L., 2019. Pyroxenite-derived Cenozoic basaltic magmatism in central Inner Mongolia, eastern China: Potential contributions from the subduction of the Paleo-Pacific and Paleo-Asian oceanic slabs in the Mantle Transition Zone. Lithos, 332, 39-54. https://doi.org/10.1016/j.lithos.2019.02.012

Patchett, P. J., White, W. M., Feldmann, H., Kielinczuk, S., & Hofmann, A. W., 1984. Hafnium/rare earth element fractionation in the sedimentary system and crustal recycling into the Earth's mantle. Earth and Planetary Science Letters, 69, 365-378. https://doi.org/10.1016/0012-821X(84)90195-X

Patchett, J., & Kouvo, O., 1986. Origin of continental crust of 1.9-1.7 Ga age: Nd isotopes and U-Pb zircon ages in the Svecokarelian terrain of South Finland. Contributions to Mineralogy and Petrology, 92, 1–12. https://doi.org/10.1007/BF00373959

Pearce, J. A., 1982. Trace element characteristics of lavas from destructive plate boundaries. Andesites, 8, 525-548.

Pearce, J. A., & Peate, D. W., 1995. Tectonic implications of the composition of volcanic arc magmas. Annual Review of Earth and Planetary Sciences, 23, 251-285.

Pearce, J. A., 2008. Geochemical fingerprinting of oceanic basalts with applications to ophiolite classification and the search for Archean oceanic crust. Lithos, 100, 14-48. https://doi.org/10.1016/j.lithos.2007.06.016

Peltonen, P., 1995. Magma-country rock interaction and the genesis of Ni-Cu deposits in the Vammala Nickel Belt, SW Finland. Mineralogy and Petrology, 52, 1–24. https://doi.org/10.1007/BF01163124

Peltonen, P., 2005. Svecofennian mafic-ultramafic intrusions. Developments in Precambrian Geology, 14, 407–441. https://doi.org/10.1016/S0166-2635(05)80010-6

Peltonen, P., Mänttäri, I., Huhma, H., & Whitehouse, M. J., 2006. Multi-stage origin of the lower crust of the Karelian craton from 3.5 to 1.7 Ga based on isotopic ages of kimberlite-derived mafic granulite xenoliths. Precambrian Research, 147, 107-123. https://doi.org/10.1016/j.precamres.2006.02.008

Pertermann, M., & Hirschmann, M. M., 2003. Partial melting experiments on a MORB-like pyroxenite between 2 and 3 GPa: Constraints on the presence of pyroxenite in basalt source regions from solidus location and melting rate. Journal of Geophysical Research: Solid Earth, 108, 1–17. https://doi.org/10.1029/2000JB000118

Polat, A., Hofmann, A. ., & Rosing, M., 2002. Boninite-like volcanic rocks in the 3.7–3.8 Ga Isua greenstone belt, West Greenland: geochemical evidence for intra-oceanic subduction zone processes in the early Earth. Chemical Geology, 184, 231–254. https://doi.org/10.1016/S0009-2541(01)00363-1 ok

Rapp, R. P., & Watson, E. B., 1995. Dehydration Melting of Metabasalt at 8-32 kbar: Implications for Continental Growth and Crust-Mantle Recycling. Journal of Petrology, 36, 891–931. https://doi.org/10.1093/petrology/36.4.891

Reagan, M. K., & Gill, J. B. 1989. Coexisting calcalkaline and high-niobium basalts from Turrialba Volcano, Costa Rica: Implications for residual titanates in arc magma sources. Journal of Geophysical Research: Solid Earth, 94, 4619-4633. https://doi.org/10.1029/JB094iB04p04619

Rudnick, R. L., 1995. Making continental crust. Nature, 378, 571. https://doi.org/10.1038/378571a0

Rudnick, R. L., Barth, M., Horn, I., McDonough, W.F., R. L., 2000. Rutile-bearing refractory eclogites: Missing link between continents and depleted mantle. Science, 287, 278–281. https://doi.org/10.1126/science.287.5451.278

Rudnick, R. L., & Gao, S., 2003. Composition of the continental crust. In: The crust, Treatise on Geochemistry, 3, 1-64.

Ruotoistenmäki, T., 2019. Adakitic plutonic rocks in the Finnish Precambrian: Evolution and areal, chemical, physical and age variations. Geological Survey of Finland, Special Publications, 102, 1-146.

Rutanen, H., Andersson, U. B., Väisänen, M., Johansson, Å., Fröjdö, S., Lahaye, Y., & Eklund, O., 2011. 1.8 Ga magmatism in southern Finland: Strongly enriched mantle and juvenile crustal sources in a post-collisional setting. International Geology Review, 53, 1622–1683. https://doi.org/10.1080/00206814.2010.496241

Rutland, R. W. R., Williams, I. S., & Korsman, K., 2004. Pre-1.91 Ga deformation and metamorphism in the Palaeoproterozoic Vammala Migmatite Belt, southern Finland, and implications for Svecofennian tectonics. Bulletin of the Geological Society of Finland, 76, 93–140. https://doi.org/10.17741/bgsf/76.1-2.005

Ryerson, F. J., & Watson, E. B., 1987. Rutile saturation in magmas: implications for Ti-Nb-Ta depletion in island-arc basalts. Earth and Planetary Science Letters, 86, 225–239. https://doi.org/10.1016/0012-821X(87)90223-8

Rämö, O. T., Vaasjoki, M., Mänttäri, I., Elliott, B. A., & Nironen, M., 2001. Petrogenesis of the post-kinematic magmatism of the Central Finland granitoid complex I; radiogenic isotope constraints and implications for crustal evolution. Journal of Petrology, 42, 1971–1993. https://doi.org/10.1093/petrology/42.11.1971

Salters, V. J., & Stracke, A., 2004. Composition of the depleted mantle. Geochemistry, Geophysics, Geosystems, 5. https://doi.org/10.1029/2003GC000597

Schärer, U., Corfu, F., & Demaiffe, D., 1997. U-Pb and Lu-Hf isotopes in baddeleyite and zircon megacrysts from the Mbuji-Mayi kimberlite: Constraints on the subcontinental mantle. Chemical Geology, 143, 1–16. https://doi.org/10.1016/S0009-2541(97)00094-6

Shand, S. J., 1943. Eruptive rocks. Their genesis, composition, classification, and their relation to ore-deposits with a chapter on meteorites. John Wiley & Sons, 1-444.

Shaw, D. M., 1970. Trace element fractionation during anatexis. Geochimica et Cosmochimica Acta, 34, 237-243. https://doi.org/10.1016/0016-7037(70)90009-8

Sobolev, A. V., Hofmann, A. W., Sobolev, S. V., & Nikogosian, I. K. 2005. An olivine-free mantle source of Hawaiian shield basalts. Nature, 434, 590. https://doi.org/10.1038/nature03411

Stephens, M. B., & Andersson, J., 2015. Migmatization related to mafic underplating and intra- or

back-arc spreading above a subduction boundary in a 2.0–1.8 Ga accretionary orogen, Sweden. Precambrian Research, 264, 235–257. https://doi.org/10.1016/J.PRECAMRES.2015.04.019

Sun, S., & McDonough, W. F., 1989. Chemical and isotopic systematics of oceanic basalts: implications for mantle composition and processes. Geological Society, London, Special Publications, 42, 313–345. https://doi.org/10.1144/GSL.SP.1989.042.01.19

Suominen, V., 1988. Radiometric ages on zircons from a cogenetic gabbro and plagioclase porphyrite suite in Hyvinkää, southern Finland. Geological Society of Finland, Bulletin, 60, 135–140.

Tang, M., Wang, X. L., Shu, X. J., Wang, D., Yang, T., & Gopon, P., 2014. Hafnium isotopic heterogeneity in zircons from granitic rocks: Geochemical evaluation and modeling of "zircon effect" in crustal anatexis. Earth and Planetary Science Letters, 389, 188-199. https://doi.org/10.1016/j.epsl.2013.12.036

Tang, M., Erdman, M., Eldridge, G., & Lee, C. T. A., 2018. The redox "filter" beneath magmatic orogens and the formation of continental crust. Science Advances, 4, 1–8. https://doi.org/10.1126/sciadv.aar4444

Tang, M., Jiang, H., Erdman, M., Costin, G., Chen, K., & Lee, C. T. A., 2019. Nb/Ta systematics in arc magma differentiation and the role of arclogites in continent formation. Nature Communications, 10. https://doi.org/10.1038/s41467-018-08198-3

Tatsumi, Y., Hamilton, D. L., & Nesbitt, R. W., 1986. Chemical characteristics of fluid phase released from a subducted lithosphere and origin of arc magmas: evidence from high-pressure experiments and natural rocks. Journal of Volcanology and Geothermal Research, 29, 293-309. https://doi.org/10.1016/0377-0273(86)90049-1

Tatsumi, Y., 2000. Continental crust formation by crustal delamination in subduction zones and complementary accumulation of the enriched mantle I component in the mantle. Geochemistry, Geophysics, Geosystems, 1. https://doi.org/10.1029/2000GC000094

Väisänen, M., Eklund, O., Lahaye, Y., O'Brien, H., Fröjdö, S., Högdahl, K., & Lammi, M., 2012a. Intra-orogenic Svecofennian magmatism in SW Finland constrained by LA-MC-ICP-MS zircon dating and geochemistry. Gff, 134, 99–114. https://doi.org/10.1080/11035897.2012.680606

Väisänen, M., Johansson, Å., Andersson, U. B., Eklund, O., & Hölttä, P., 2012b. Palaeoproterozoic adakite-and TTG-like magmatism in the Svecofennian orogen, SW Finland. Geologica Acta, 10, 351–371. https://doi.org/10.1344/105.000001761

Wernicke, B., Clayton, R., Ducea, M., Jones, C. H., Park, S., Ruppert, S., Phinney, R., 1996. Origin of High Mountains in the Continents: The Southern Sierra Nevada. Science, 271, 190–193. https://doi.org/10.1126/science.271.5246.190

Xu, W., Gao, S., Wang, Q., Wang, D., & Liu, Y., 2006. Mesozoic crustal thickening of the eastern North China craton: Evidence from eclogite xenoliths and petrologic implications. Geology, 34, 721. https://doi.org/10.1130/G22551.1

Zack, T., Kronz, A., Foley, S., & Rivers, T., 2002. Trace element abundances in rutiles from eclogites and associated garnet mica schists. Chemical Geology, 184, 97–122. https://doi.org/10.1016/S0009-2541(01)00357-6

Zandt, G., Gilbert, H., Owens, T. J., Ducea, M., Saleeby, J., & Jones, C. H., 2004. Active foundering of a continental arc root beneath the southern Sierra Nevada in California. Nature, 431, 41–46. https://doi.org/10.1038/nature02847